PREVENTING DELAYED CRACKS IN SUS304 DEEP DRAWN CUPS USING EXTREME BLANK HOLDING FORCES AIDED BY NANOLUBRICATION

MUHAMMAD SHAFIQ BIN IBRAHIM

ENGINEERING FACULTY
UNIVERSITY OF MALAYA
KUALA LUMPUR

2020

PREVENTING DELAYED CRACKS IN SUS304 DEEP DRAWN CUPS USING EXTREME BLANK HOLDING FORCES AIDED BY NANOLUBRICATION

MUHAMMAD SHAFIQ BIN IBRAHIM

DISSERTATION SUBMITTED IN FULFILMENT OF THE REQUIREMENTS FOR THE DEGREE OF MASTER OF ENGINEERING SCIENCE

ENGINEERING FACULTY
UNIVERSITY OF MALAYA
KUALA LUMPUR

2020

UNIVERSITY OF MALAYA

ORIGINAL LITERARY WORK DECLARATION

Name of Candidate: MUHAMMAD SHAFIQ BIN IBRAHIM

Matric No: KGA160

Name of Degree: Master of Engineering Science

Title of Project Dissertation: Preventing Delayed Cracks in SUS304 Deep Drawn Cups using Extreme Blank Holding Forces Aided by Nanolubrication.

Field of Study: Engineering Design (Engineering & Engineering Trades)

I do solemnly and sincerely declare that:

(1) I am the sole author/writer of this Work;

(2) This Work is original;

(3) Any use of any work in which copyright exists was done by way of fair dealing and for permitted purposes and any excerpt or extract from, or reference to or reproduction of any copyright work has been disclosed expressly and sufficiently and the title of the Work and its authorship have been acknowledged in this Work;

(4) I do not have any actual knowledge nor do I ought reasonably to know that the making of this work constitutes an infringement of any copyright work;

(5) I hereby assign all and every rights in the copyright to this Work to the University of Malaya ("UM"), who henceforth shall be owner of the copyright in this Work and that any reproduction or use in any form or by any means whatsoever is prohibited without the written consent of UM having been first had and obtained;

(6) I am fully aware that if in the course of making this Work I have infringed any copyright whether intentionally or otherwise, I may be subject to legal action or any other action as may be determined by UM.

Candidate's Signature   Date:

Subscribed and solemnly declared before,

Witness's Signature   Date:

Name:

Designation:

ABSTRACT

This study was to investigate the formation and reformation of delayed cracks of SUS304 cylindrical drawn cups under elevated blank holding force (BHF) from 8~32 kN with 1~3 wt% SiO_2 nanolubricants concentrations. The widest crack-free BHF range i.e. from 29 ~ 31 kN was determined for 2 wt% of SiO_2 in the experiment. Delayed cracks were also observed below and beyond this BHF range. There was an increment of frictional force at the cup flange region when entering the crack-free BHF range, as proven by the rebound in sidewall thickness, relative intensity of α'-martensite, elongated height and drawing force beyond 28 kN. The crack reformation after exiting crack-free BHF range was due to the worsened nanolubricant tribological performance when undergoing excessive pressure, hence, allowing high friction induction. The $\alpha'-$martensite had the highest relative intensity (%) at 93.7 % for BHF = 28 kN, leading to the delayed cracks. The relative intensity slightly decreased after the peak within the crack-free range with intensities ranging from 83.8 ~ 89.9 % before experiencing a sharp decrease to 50.7 % for 32 kN leading to the reformation of the cracks again. Residual stresses were developed along the outer surface of the cup due to the unbending of the material when the material left the draw die profile, hence, the increase in frictional force in the radial direction along the flange surfaces reduced the circumferential tensile residual stress of the cup, particularly at 80 % cup height. The elimination of the cracks was attributed to the decrease in intensity of the α'-martensite and the lower tensile stress gradient. The minimum BHF required for eliminating the cracks was hardly altered by the increase in concentration of SiO_2.

Keywords: Delayed crack; Deep drawing; Metastable austenitic stainless steel; Nanolubricant; Residual stress.

ABSTRAK

Kajian ini menyiasat pembentukan dan pembentukan semula retakan pada spesimen cawan berbentuk silinder yang diperbuat daripada keluli tahan karat 304 bawah pengaruh BHF (8 – 32 kN) bersama 1-3 wt% SiO_2 kepekatan campuran pelincir nano. Julat BHF bebas retak terbesar   adalah 29 ~ 31kN, diperolehi dengan menggunakan 2wt% SiO_2. Keretakan berlaku di bawah dan diluar julat BHF ini. Terdapat peningkatan dalam kadar daya geseran di bahagian hujung tepi spesimen sebelum memasuki julat bebas retak, seperti dibuktikan melalui perubahan pola ketebalan dinding, intensiti α'-martensit, permanjangan ketinggian spesimen dan daya yang dikenakan dalam operasi penarikan selepas melepasi BHF=28kN. Pembentukan semula retakan selepas melepasi julat bebas retak berpunca daripada prestasi tribologi pelincir nano yang telah merosot apabila berada dibawah kadar tekanan yang amat tinngi lalu menyebabkan pembentukan daya geseran yang tinggi. Peratus α'-martensit tertinggi dengan intensity 93.7 % direkodkan untuk BHF = 28kN, yang membawa kepada keretakan spesimen. Intensiti α'-martensit kemudiannya menurun selepas julat bebas retak dengan intensity antara 83.8 ~ 89.9% sebelum mengalami penurunan mendadak kepada 50.7% untuk BHF=32kN yang membawa kepada pembentukan semula keretakan. Disebabkan baki tekanan dihasilkan sepanjang permukaan luar spesimen cawan apabila berlaku pembengkokkan bahan sewaktu pergerakan keluar dari acuan, peningkatan kecil geseran sepanjang permukaan hujung tepi spesimen menyebabkan pengurangan tegangan baki tekanan di keliling spesimen, iaitu di ketinggian 80%. Penghapusan retakan disebabkan sedikit penurunan α'-martensit dan kecerunan baki tekanan yang rendah. BHF minimum yang diperlukan untuk menghapuskan retakan tidak banyak dipengaruhi oleh peningkatan kepekatan SiO_2 .

Kata kunci: Tangguhan retakan; Operasi penarikan dalam; Keluli tahan karat; Metastable Austenit; Pelincir nano; Baki tekanan.

ACKNOWLEDGEMENTS

I would first like to express my sincere gratitude to my research advisors Dr Tan Chin Joo and Dr Mohd Ridha Bin Muhamad of the Department of Mechanical Engineering, Faculty of Engineering at University of Malaya for the continuous support of my Master study and related research, for their patience, motivation, and immense knowledge. Their guidance helped me in all the time of research and writing of this thesis. I could not have imagined having a better advisors and mentor for my Master study.

My sincere thanks to the laboratory and workshop technicians at Faculty of Engineering, who have provided support and assisted me whenever I needed help in using the facilities during experiment execution. Without their precious support it would not be possible to conduct this research.

I also would like to thank my fellow lab mates for the sleepless nights we were working together before deadlines, and for all the fun we have had in the last 2 years.

Last but not the least, I would like to thank my family: my parents and to my brothers and sister for supporting me spiritually throughout writing this thesis and my life in general.

TABLE OF CONTENTS

LIST OF FIGURES

LIST OF TABLES

LIST OF SYMBOLS AND ABBREVIATIONS

SUS	Stainless Steel
°C	Degrees Celsius
°K	Degrees Kelvin
α	Alpha
BHF	Blank Holding Force
Wppm	Weight parts per million
wt%	Weight percent
SiO_2	Silicon Oxide
mm/s	Millimeter per second
Nm	Nanometers
°	Degree
FCC	Face-Centered Cubic
BCC	Body -Centered Cubic
HCP	Hexagonal Close-Packed
AISI	American Iron and Steel Institute
FEM	Finite Element Method
SFE	Stacking Fault Energy
Ni	Nickel
Cr	Chromium
Mn	Manganese
Al	Aluminium
Mg	Magnesium
Si	Silicon
Mo	Molybdenum

Cu	Copper
O	Oxygen
Zn	Zinc
Zr	Zirconium
Ce	Cerium
PC	Pre-stressed Concrete
MPa	Mega Pascal
HV	High Voltage
Hz	Hertz
kN	Kilo Newton
D_p	Punch Diameter
D_d	Die Diameter
XRD	X-Ray Diffraction
EDM	Electrical Discharge Machining
LDR	Limited Drawing Ratio
MQL	Minimum Quantity Lubrication

CHAPTER 1: INTRODUCTION

1.1 Introduction

This chapter discusses initially the background includes the current application of deep drawing operation of SUS304 metastable austenitic stainless steel and its problem like delayed cracking. This chapter also covers the research significance on industry and research field particularly in metal forming along the research objectives and motivation.

1.2 General background

Metastable austenitic stainless steels such as SUS304 are increasingly used to manufacture variety of kitchen utensils like sinks, cooking pots and some applications of automotive components, for instance, filter connectors and battery containers for hybrid vehicles due to their potential to be deep drawn into different shapes and high energy − absorbing capacity (Chen, Fuh-Kuo & Pao-Ching Tseng, 2005.

In addition, in medical devices industry, SUS304 has become an attractive material to manufacture different kinds of medical applications like housing and casing components for cochlear, cardio, and implantable medical devices because it offers unique characteristics like high corrosion resistance, good formability and antibacterial properties. However, the main reason that makes SUS304 as the most suitable material to manufacture life-saving equipment is the ability to manufacture parts with various geometries or shapes that perfectly match with the stringent requirement for medical use through deep drawing operation. Currently, SUS304 accounts for 2/3 of the world's stainless-steel production.

Figure 1.1: Stainless steel products made from deep drawing operation

The deep drawing is a sheet metal working process which uses the combination of tensile and compressive forces to stretch metal. This metal forming operation has been used and upgraded since the end of the 19th century due to its ability to convert the sheet metal into various complex shapes or geometries through a simple process (Simões, 2012). Figure 1.2 shows the illustration of deep drawing operations. In this process, the sheet metal blanks are drawn deeply into a forming die using the mechanical action of a punch into a desired shape and thickness. This metal forming operation is known as deep drawing due to the depth of the product manufactured which is equal to or larger than its radius.
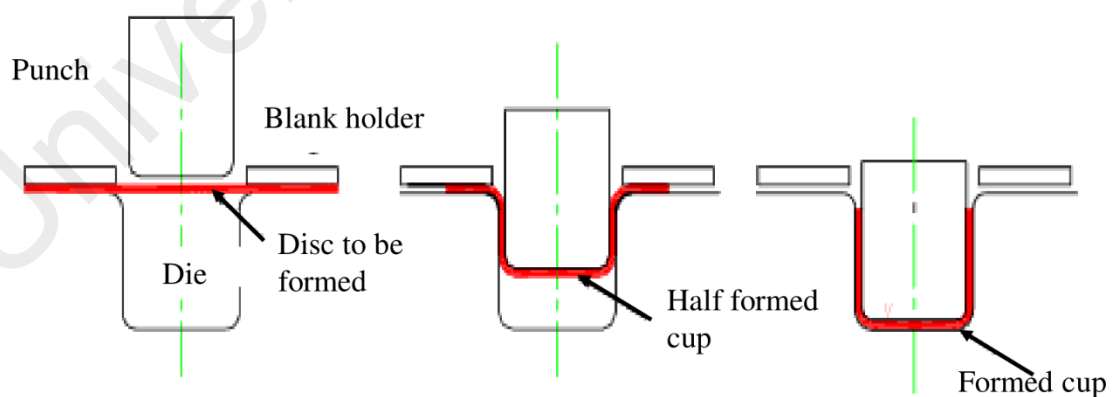
Figure 1.2: Deep drawing operations

However, parts that are made from metastable austenitic stainless steels, particularly low nickel content grades are prone to incur a harmful phenomenon of delayed cracking (Papula, 2015) which often occurs unexpectedly in successfully formed components after an incubation period of a few minutes, hours, days or even weeks after undergoing a metal forming operation (Huang & Altstetter, 1991), for example, a deep drawing.
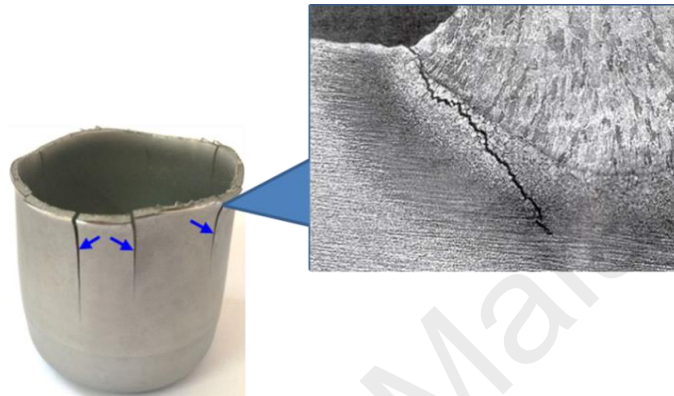
Figure 1.3: Delayed cracks appearance in successfully formed stainless steel cup (Bill Lucas., 2000)

It is established that the appearance of this delayed cracking phenomenon in deep drawn steels components can be directly related to the coexistence of strain-induced α'-martensite, the presence of hydrogen in material and also the tensile residual stress (Berrahmoune, Sophie Berveiller, Karim Inal, & Etienne Patoor, 2006). However, the effect of hydrogen is not studied in this study. Hydrogen exists as an impurity in SUS304. This element been absorbed from the environment during the manufacturing process or from water contained in the raw materials. However, its content will not change under BHF enhancement. Therefore, the elimination of fractures will not due to the decrease in hydrogen content.

The deep drawing is currently known as the most popular metal forming method available to manufacturers due to its potential in producing high volumes. As the demand of higher strength steels using deep drawing operation increases the alternatives of

controlling delayed fracture of drawn stainless steels components become one of the manufacturing industry priorities. The timing for the fracture's occurrence cannot be predicted, hence, this could affect product's quality and most alarmingly its unfavourable risk to the users. Furthermore, the defect needs repairs that are often costly. Hence, a number of methods in mitigating delayed cracking in stainless steels applications have been studied such as heat treatments at 400°C (Papula, 2015), tool clearance minimization through ironing (Yang, Xu, & Xing, 1990), redrawing process (Frehn & Bleck, 2003) and nickel addition in stainless steels (Papula, Talonen, Todoshchenko, & Hänninen, 2014). However, besides the effectiveness in preventing fractures, the studied alternatives have significant drawbacks like annealing requires high cost and surface quality tend to affect under high temperature (Papula, 2015). Additionally, ironing process is proven to be effective in reducing residual stress, however advanced lubrication and costly tools require to accomplish this method (Yang, Xu, & Xing, 1990). Therefore, this study will contribute to a new method and mechanism in eliminating delayed cracking issues through different parameters combinations and series of experiments. Additionally, this research will shed some light on improving the effectiveness of deep drawing, so that this method could be widen used in industry.

1.3 Importance of study

The findings of this study will benefit the stainless-steel manufacturing industry particularly in relation to deep drawn product. Deep drawing is one of the most popular metal forming industries due to its vast benefits especially when manufacturing large volumes, because unit cost decreases considerably as unit count increases. However, the unfavourable phenomenon of delayed cracking always poses a serious issue especially in terms of the safe application of stainless steels product like lightweight structures in the automotive industry. A number of studies have proposed several methods in mitigating

fracture through heat treatment (Papula, 2015) and nickel addition in steels (Papula, Talonen, Todoshchenko, & Hänninen, 2014). These methods are proven to be effective in eliminating fracture, however the high cost in providing heat treatment facilities and volatile price of nickel have made researchers to seek other alternatives that are much more reliable and cost-saving. Hence, this study will contribute to a new method and mechanism in solving delayed cracking issue through different combinations of parameters and series of experiments.

1.4 Motivation

This section clarifies 3 factors that motivate the research undertaken in this study. First, the metastable austenitic stainless steel particularly SUS304 has become the most favorable and versatile material in manufacturing industry due to its excellent forming ability characteristics and its mechanical properties. Second, the deep drawing is currently known as the most popular metal forming method available to manufacturers due to its potential benefits in many ways like increasing the metal forming capabilities and reducing operation cost unlike bulk forming operations for examples rolling, forging, extrusion and wire drawing which involve high operation cost. Third, there is a need to increase the understanding and seek effective solutions regarding the susceptibility of SUS304 components to delayed cracking after undergoing a forming operation like deep drawing.

1.4.1 Vast potential of stainless steel SUS304 and deep drawing operation in manufacturing industry.

Austenitic stainless steels particularly SUS304 has become the most versatile and largest material used in various manufacturing industries, approximately 2/3 of the world's stainless-steel production due to its characteristic in possessing an excellent combination of strength and elongation that is good to be severely deep drawn. This

property has resulted in SUS304 being the dominant grade used in many applications such as sinks, cooking pots and some medical applications like implantable medical devices using deep drawing as an ideal metal forming method.

Besides, due to its advantage of producing high volumes, and the unit cost reduces considerably as unit count increases and produces the desired shape by a simple process, deep drawing has become the most popular metal forming method available to manufacturers. Additionally, deep drawing which is in sheet metal forming category is much more preferable than bulk metal forming like rolling, forging, extrusion and wire drawing because no heating is involved throughout the process, hence furnace, fuel and electricity costs can be effectively minimized. Other sheet metal forming operations like bending, shearing and also deep drawing are done at room temperature or slightly above room temperature while the bulk forming operations are mostly done in hot working conditions. Deep drawing is also one of the best techniques in metal forming because it increases forming capabilities which are ideal for products that require significant strength and minimal weight. Automotive industry implements this metal forming operation to deep drawn components like outer and inner car body panels, stiffeners and fenders.
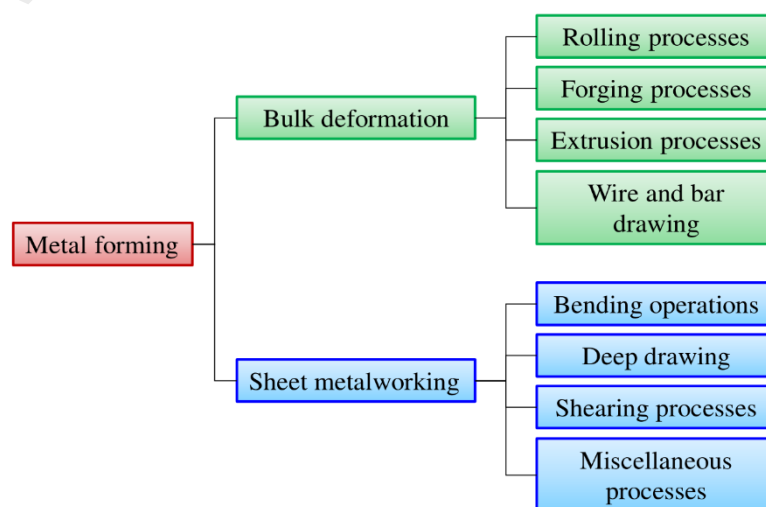
Figure 1.4: General classification of metal forming processes (Narayanan)

However, the phenomenon of delayed cracking is tend to occur after deep drawing operations of SUS304 product (Papula, 2015). This rejectable defect is dangerous, as fracture can lead to catastrophic events if they are not recognized and repaired prior to a part entering the service especially for manufacturers or contractors that use steel in critical applications like automotive, medical and offshore industries. The problem gets worsened because the incubation period till fracture may vary in the order from second, days or even weeks, where many issues may arise in the safe application of stainless steel (Guo, 2008). Additionally, this defect needs repairs that are often costly. Therefore, this study will shed some light on how to avoid any predicaments that might arise when dealing with SUS304 material application using deep drawing operation.

1.4.2 Needs in finding reliable and efficient methods in mitigating problems related to deep drawing of SUS304.

There have been various attempts by researchers to study and evaluate the possible factors contributing to delayed cracking, including strain-induced α'-martensite, residual stresses and the presence of hydrogen in material. However, the significance of the various features, as well as the mechanism and kinetics related to this phenomenon still remain unclear and need further research to fill the knowledge gap and enhance understanding in this field.

A number of researchers have conducted studies on how to prevent delayed cracking in austenitic stainless steel for example, through heat treatments at 400°C. (Papula, 2015) proved that by applying certain degree of heat on austenitic stainless steel, the hydrogen content was reduced effectively, which in turn, increases the austenite stability, which eventually will decrease the possibility of fracture to occur. Ironing and redrawing processes are also proposed. Regardless of this processes efficiency in reducing the risk

percentage for fracture occurrence, the high cost in providing heat treatment facilities and ironing tools force the manufacturers to find other profitable pricing alternatives.

Therefore, an investigation of new mechanism used and a combination of parameters in series of experiments in this study will help achieve this. In addition, such an investigation provides an opportunity to study how the factors influence the fracture occurrence and the austenitic stainless steels durability.

1.5 Objectives

1.5.1 Aim of study

This research is to clarify the reasons for high susceptibility of the most stable austenitic stainless steel of SUS304 to delayed cracking under elevated BHF using different nanolubricant concentrations at a limiting drawing ratio, and to investigate the influence of austenite and α'-martensite stability and also residual stress contained in the samples.

1.5.2 Objectives

1. To determine the blank holding force (BHF) required for crack free region in SUS304 under the influence of different SiO_2 concentration of 1,2 and 3 wt%.

2. To investigate the mechanism of delayed cracks in SUS304 cylindrical drawn cups under elevated blank holding forces (BHFs) of 8~32 kN with the application of $1 \sim 3$ wt% SiO_2 nanolubricant.

3. To investigate the influence of martensitic transformation and residual stress contained in the samples drawn under elevated blank holding forces (BHFs) of 8~32 kN with the application of $1 \sim 3$ wt% SiO_2 nanolubricant.

1.6 Research scope

The study discusses the reasons for the occurrence of delayed cracking phenomenon in most stable austenitic stainless steel, particularly SUS304 under elevated BHF of 8~32 kN with nanolubricants containing $1 \sim 3$ wt% SiO_2 concentrations at a limiting drawing ratio of 2.12 which is a drawing ratio that can be successfully drawn without cracking. The deep drawing operation was used throughout the experiment using a 25-ton press at a punch speed of 1.1 mm/s. A cylindrical punch and circular die with 34 and 37.4-mm diameter respectively were used, giving a cylindrical cup shape of the test sample. Cylindrical and square cup drawing are the most popular and simple deep drawing types. However, in this research, cylindrical type was chosen due to its convenience and less critical property compared to square cup drawing as there is a tangential symmetry in cylindrical cup drawing which enables an analysis of only a wedge-shaped sector of the metallic sheet (Başpınar & Akkök, 2016).

Laser-cut circular SUS304 blanks with the initial thickness and diameter of 1.17~1.20 mm and 72 mm respectively were used in the test. The aspects looked into were strain-induced martensitic transformation, tensile residual stress along the drawn cup's outer surface, the number of cracks and time taken for the first crack to appear with different concentrations of SiO_2 and BHFs, the change in cup wall thickness under different BHFs, the average peak and valley point heights along the cup edge measured from the bottom for different BHFs and the forming loads for different BHFs.

1.7 Outline of the thesis

This thesis comprises 5 chapters. The chapter begins with Chapter 1 which covers the general background and current issues regarding the research area and latest information surrounding the issues. This chapter also includes the research significance, the overall objectives of the study, the research scope of what exactly to explore and also how the research benefits in improving the existing knowledge in the field and provides insights to a consumer-relevant questions.

Chapter 2 is the literature review. This chapter describes the critical synthesis of previous research regarding the study area including a summary, description and critical evaluation of works in relation to the research problems being studied.

Chapter 3 reflects the methodology used that presents the systematic and theoretical analysis of the methods used to integrate the different research components in a logical and coherent way, thereby, offering methods to solve the research problems effectively.

Chapter 4 is the main section where the outcomes of the study obtained upon the methodology applied are presented. This chapter discusses the results of analysis and their interpretation of in order to answer the research problems being investigated, and to explain any new understanding on the problem after taking the outcomes into account.

Lastly, Chapter 5 focuses on summary of the main points from the whole research, specifically the research problem statement. At the end of this chapter, few recommendations are proposed, in relation to the problems found throughout the study.

CHAPTER 2: LITERATURE REVIEW

2.1 Introduction

In this second chapter, the theoretical background regarding the deep drawing operations and failure like delayed cracking, factors influencing fracture in deep drawn stainless steel product and research methods in mitigating delayed cracking that have been studied by previous researchers are provided.

2.2 Deep drawing process

Deep drawing is a manufacturing process that is used largely in the forming of sheet metal in which a flat sheet metal is radially drawn into a forming die by the mechanical action of a punch (Papula, 2015). This metal forming operation has been used and upgraded since the end of the 19th century due to its ability to convert the sheet metal into various complex shapes or geometries through a simple process (Simões, 2012). The operation is considered 'deep' drawing as the depth of the drawn part equal to or larger than its diameter.

In details, deep drawing is a large productivity manufacturing process that is extensively used in industries like the machinery and automotive components, to manufacture products made from metallic flat rolled sheet or also known as blank. This process requires three main tools: punch, die and blank holder. The common punch in cylindrical shape is used to move the sheet into forming die cavity and deform the sheet to its final shape. The final shape of the product is defined by the geometry of the forming die and punch. The blank holder is an ultimately important tool as it controls the sheet metal flow (Sniekers, 1996) by pressing the outer section of the blank, known as flange against the die during the drawing process.

Figure 2.1 (Simões, 2012) shows the deep drawing process for a cylindrical cup. The figure illustrates the successive steps from an originally circular blank to the product with its final drawn shape. The flat blank sheet is sandwiched between the blank holder at the top and the die placed underneath the sheet. In the first step, the blank holder is set on the blank. During the second step, the punch is moved downwards to ram and move the sheets through the die's cavity until the final shape of the sheet is successfully deformed. Finally, the punch is pulled back and the blank holder removed. The deformed sheet is then removed from the die's cavity. However, the formed stainless-steel products that are made from deep drawing operation are susceptible to a harmful phenomenon known as delayed cracking. A number of researches have been conducted to study the details regarding this unfavorable defect as explained in the next section.
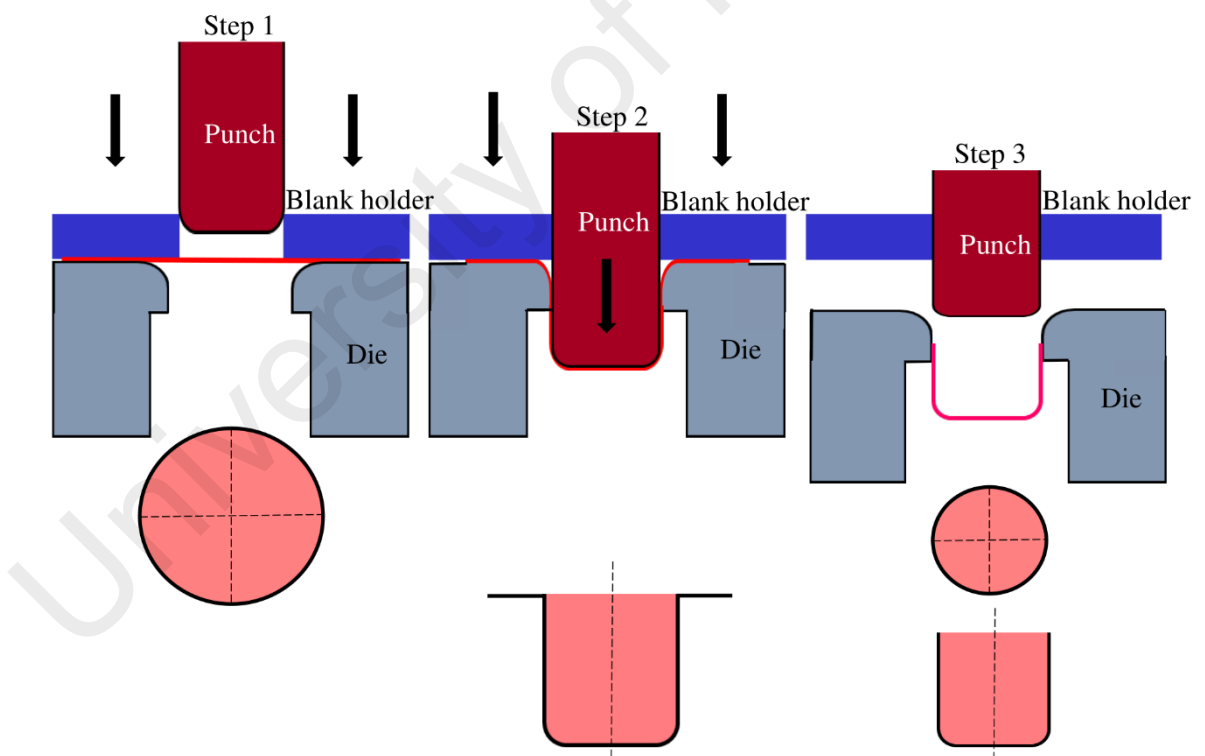
Figure 2.1: Deep drawing process for a cylindrical cup (Simões, 2012)

2.3 Delayed cracking of austenitic stainless steels in deep drawing operations

The stainless steel forming process using deep drawing at room temperature tends to cause unfavorable defects like the phenomenon of delayed or longitudinal cracking along the side walls of the cups that may occur unexpectedly in successfully formed components after an incubation period of a few minutes, hours, days or even weeks (Huang & Altstetter, 1991; Jung et al., 2017; Yuying, Chunfeng, & Hongzhi, 1992).

In general, delayed fracture is formed at the cylindrical cup edge and developed linearly in the depth direction. The successful deep drawn components fracture in a matter of time without external applied stress. The unpredictable incubation time till rupture raises many problems in the safe application of austenitic stainless steel. The incubation time before cracking's appearance is mainly due to the hydrogen diffusion to high tensile stress regions. The severity of cracks depends upon the hydrogen accumulation in that region. It is established that the appearance of this phenomenon in these steels can be directly related to the coexistence of hydrogen in the material , strain-induced α'-martensite and tensile residual stress (Berrahmoune, Sophie Berveiller, Karim Inal, & Etienne Patoor, 2006).

2.3.1 Effect of internal hydrogen

Delayed cracking or internal hydrogen embrittlement, is mainly caused by the internal hydrogen, as the number of fractures appearing in deep drawn cups has been observed to depend directly on the amount of hydrogen dissolved in the steel (Sumitomo, 1987; Zhang et al., 2012; Zhang, Wen, Imade, Fukuyama, & Yokogawa, 2008).

Austenitic stainless steels contain a small amount of hydrogen, which is an inevitable impurity accumulated during the steel production process. The steel manufacturing processes like cathodic electrolytical cleaning, bright annealing and even water contained

in the raw material prone steels to hydrogen absorption. Even the tiniest amount of hydrogen dissolved in steels is sufficient to cause delayed cracking (Papula, 2015).

The presence of α′-martensite, which is an intrinsically more brittle and harder phase than austenite, offers potential fracture initiation sites and can enhance markedly the embrittling effect of hydrogen (HÄNNINEN & HAKARAINEN, 1980). α′-martensite serves as a fast diffusion path for hydrogen to fracture initiation sites, due to the diffusivity of hydrogen in BCC phases, like α′-martensite of ferrite, is much greater than in FCC phases, like austenite (Kanezaki, Narazaki, Mine, Matsuoka, & Murakami, 2008; San Marchi, Somerday, Tang, & Schiroky, 2008). α′-martensite phase accelerates hydrogen diffusion, however the hydrogen solubility in α′-martensite is much lower than in austenite. Hydrogen tends to accumulate in the phase boundary between martensite and austenite, resulting in local strain and increasing delayed cracking initiation (Berrahmoune, Sophie Berveiller, Karim Inal, & Etienne Patoor, 2006).

Hydrogen can severely deteriorate the fracture initiation and propagation resistance of high – strength alloys by facilitating the microscopic processes that constitute fracture initiation and advance. Diffusible hydrogen in the crystal lattice prone to gather in the highly stresses zone of fracture tip, under the influence of a stress gradient, hence increasing crack propagation as shown in Figure 2.2 (Gangloff, 2003; Wang et al., 2012). Hydrogen can be transported by diffusion and mobile dislocations. The existence of stress causes a redistribution of dissolved hydrogen from the surrounding microstructure to the crack-tip fracture process region, which can cause strong gradients in hydrogen concentration and stress around the crack tip. Hydrogen gathers in the crack-tip fracture process region under the influence of two driving forces. First, the hydrogen concentration in interstitial lattice sites is enhanced proportionally to an exponential dependence on hydrostatic stress that dilates the lattice. The tensile stress locally increases

the hydrogen solubility. Secondly, hydrogen gathers at the crack tip because of the trapping associated with the large density of dislocations presence due to intense plastic deformation (Gangloff, 2003; Kovalev, Wainstein, Mishina, & Zabilsky, 2002).

Hydrogen-enhanced localized plasticity (HELP) model has been proposed as an important mechanism of hydrogen degradation in austenitic stainless steels. According to HELP, dissolved hydrogen in stainless steels can increase dislocation mobility and planar slip, resulting in heterogeneously localized plastic strain and stress concentrations sufficient to allow subcritical crack growth. In the zones of large hydrogen concentration, the flow stress is reduced and slip occurs at stresses well below those needed for plastic deformation in other parts of the sample, *i.e.,* slip localization takes place in the vicinity of the crack tip (Martin et al., 2011; Pan et al., 2003). This results in high localized failure by ductile processes, while the macroscopic deformation remains small due to macroscopic ductility reduction (Birnbaum & Sofronis, 1994; Lai, Tsay & Chen, 2013; Robertson, 1999).
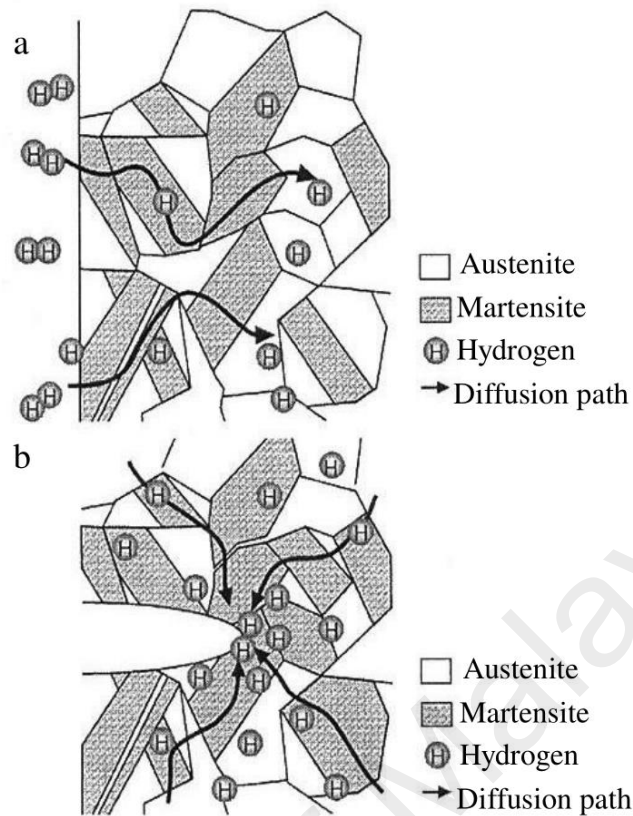
Figure 2.2: Schematic illustration of hydrogen diffusion path from surface (a) and near a crack tip (b) (Kanezaki et al., 2008).

2.3.2 Effect of strain-induced α′-martensite

After cold forming at room temperature, the unstable austenite (face-centered –cubic :FCC) contained in these steels tends to transform to thermodynamically more stable α′-martensite (body-centered-cubic :BCC) (Zinbi & Bouchou, 2010). This martensitic transformation increases the steels work-hardening rate, which is desirable for high formability, because the onset of necking is delayed, causing larger strains (Huang, Matlock, & Krauss, 1989; Talonen, 2007).

There are two martensite phases exist in austenitic stainless steels, hexagonal close-packed (HCP) ε-martensite and body – centered cubic (BCC) α′-martensite. ε-martensite is primarily known as intermediate (precursor) phase reaching its largest volume fraction

at a relatively low strain before transforming to α′-martensite at a higher strain (Lo, Shek, & Lai, 2009). Hence, only α′-martensite at a higher strain is observed in this study.

A study characterized the effect of strain-induced martensite on deformation behavior of SUS304 stainless steel (Papula, 2015). They reported that the strain rate sensitivity and strain hardening rate are correlated with the strain-induced transformation rate. However, delayed cracking is more likely to occur when the amount of strain-induced α′-martensite increases.

The presence of α′-martensite is a necessary prerequisite for delayed cracking to occur in austenitic stainless steels with typical internal hydrogen concentrations (<5 ppm) (Berrahmoune, Sophie Berveiller, Karim Inal, & Etienne Patoor, 2006). During deep drawing operation, the flange portion of the cup is subjected to high compressive stresses when the material flows into the die cavity. The highest stress value is located along the cup's circumference edge. Therefore, the largest amount of α′-martensite forms along the cup edge where the cracks initiate.

2.3.3 Effect of residual stress

Residual stresses generated during deep drawing also contributes to delayed cracking (Fratini, Pasta, & Reynolds, 2009; Yuying et al., 1992). Residual stresses introduced in a deep drawn cup are mainly caused by the unbending of the material when it leaves the draw die profile (Hong et al. 1961).

High heterogeneous residual stress state is an internal stress which remains in a body that is stationary and at equilibrium with its surroundings. The presence of residual stress affects the part fatigue strength, causes stress cracking corrosion, or leads to dimensional changes after the machining of the formed products (Ragab & Orban, 2000). Residual stresses emerge from the material elastic response to an inhomogeneous distribution of

non-elastic strains. All metal forming processes like forging, extrusion, rolling and deep drawing involve the induction of residual stresses in the material. Residual stress, which is the interaction of deformation, microstructure and temperature, is often created by inhomogeneous plastic strain levels at different locations of the product (Wang & Gong, 2002). The dissimilarity in the actual strain level in different regions may be attributed by several reasons, including a difference in strength between the co-existent phases in the material, due to die geometry or constraints from the gripping force on the workpiece, or by temperature gradients (Wang & Gong, 2002).

Residual stresses are also generated in metallic materials by phase transformations. Plastic strains are inhomogeneously divided between the phases because of the constraining effect of the stronger phases against the weaker ones. In metastable austenitic stainless steels, martensitic transformations develop as a response to plastic deformation, in which the unstable austenite (face-centered –cubic: FCC) is partially transformed to thermodynamically more stable α'-martensite (body-centered-cubic: BCC). The strain-induced martensitic transformation creates local strain fields, hence causing a varying internal stress in both phases (Berrahmoune, Berveiller, Inal & Patoor, 2006; Withers, Bhadeshia, & Technology, 2001). Martensitic transformation is a diffusionless shear process, which is accompanied by a volumetric change and shear strains. The specific volume of α'-martensite is about 2% higher than austenite (Taran, Daymond, & Schreiber, 2004). The α'-martensite phase has a greater yield strength, where hardness has a larger stress level than the austenite (Juho Talonen, 2007).

Residual stress comprises of macro and microstress components. Macrostresses generate primarily by the inhomogeneous plastic deformation at different regions of a formed component, varying slowly on a scale that is larger than material's microstructure. Microstresses, which vary on the scale of the material's microstructure, are created by the

imperfections in the crystal lattice and inhomogeneous partitioning of plastic strain between different phases, because of the constraining effect of the stronger phase against the weaker ones. The degree of plastic deformation in the phases is different because of the differences in yield strength: the softer phase starts to yield earlier and undergo greater plastic strains. In previous studies on plastically deformed dual-phase materials, the residual microstresses are compressive in the softer phase and tensile in the harder phase (Berrahmoune et al., 2004; Johansson & Odén, 2000; Lei, Masahide, Yoshiaki, Yukio, & Steel Research, 2007; Taran et al., 2004).

2.3.4 Low-nickel austenitic stainless steels

As mentioned in section 2.3.1, hydrogen is considered as the main factor causing delayed cracking because the number of fractures appearing in deep drawn cups has been observed to depend directly on the amount of hydrogen dissolved in the steel (Sumitomo, 1987; Zhang et al., 2012; Zhang et al., 2008). In addition to the effect of hydrogen, the degree of localized deformation and macroscopic ductility in austenitic stainless steels is highly dependent on the nickel content (Zinbi & Bouchou, 2010), as nickel plays a significant role in the deformation mechanism that affect hydrogen-assisted fracture (Kanezaki et al., 2008; ZHANG et al., 2012b). Low nickel steels are found to be susceptible to delayed cracking (Davis, 1994, 2000; McGuire, 2008) as insufficient nickel content enhances localized deformation and reduces the austenite stability hence, increasing the susceptibility to delayed cracking.

The nickel enhances austenite stability and stacking fault energy (SFE), which causes cross slip and consequently minimizes planar slip participation in fracturing to increase ductility. Stacking fault energy describes the plastic deformation behavior of the material, the ability of dislocations in a crystal to glide onto an intersecting slip plane (Berrahmoune, Sophie Berveiller, Karim Inal, & Etienne Patoor, 2006). The lower the

SFE of the austenitic stainless steel, the smaller is the austenite stability. The SFE decreases with the increasing of Cr content up to levels of 10-15% Cr (Berrahmoune, Sophie Berveiller, Karim Inal, & Etienne Patoor, 2006). Nickel strongly increases the SFE up to about 12 % Ni content, while at higher contents the increase is comparatively small. Therefore, high nickel steels are usually more resistant to hydrogen-assisted fracturing. However, most commercially available SUS 304 grades contain a minimum of around 8% nickel and it is not a sound practice to modify the nickel composition on account of its high and unstable market price.

In 2009, approximately 60.9% of nickel production was used for stainless steel manufacturing (Pariser, 2010). However, the rising cost of nickel forces manufacturers and users of stainless steels to find low-nickel alternatives for conventional nickel containing stainless steel grades.

There are three common elements that can substitute the role of nickel in achieving austenitic microstructure; carbon, nitrogen and manganese. According to ISSF Annual Review 2013, the global market share of low-nickel Cr-Mn stainless steels has been persistently increasing, at 15-20%. Although manganese is known as the austenitic stabilizer, another element has to be added together because the addition of Mn alone is insufficient to stabilize the austenite phase, especially in the presence of strong ferrite stabilizer element like chromium (Milititsky et al., 2008). Hence, the Cr content in low – nickel grades has to be lessened which has a bad consequence on corrosion resistance. However, the addition of Mn will maximize the nitrogen solubility in the liquid steel, hence, increasing the austenite fraction formed during solidification. Nitrogen has been proven to be an effective austenite stabilizer and also has a good effect on the pitting corrosion resistance (Simmons, 1996). Additionally, the addition of Cu in low-Ni austenitic stainless steels will stabilize the austenitic phase and also improve their

formability (Sibanda, Vismer, & Knutsen, 1994) (Gonzalez et al., 2003). Regardless of their similar mechanical properties and greater yield strength, in comparison to the 300-series grades, the Nitrogen-Manganese-Chromium alloyed austenitic stainless steels provide a lower cost alternative for the conventional austenitic grades.

2.4 Preventing delayed cracking

The impacts of delayed cracking have been observed, for example, in high strength bolts, pre-stressed concrete (PC) steel bars, reinforcing rods and stainless steel clamps after undergoing bending forming process (Akiyama, 2012). Therefore, as the demand of strength steels increases, the alternatives of controlling delayed fracture of stainless steels become one of manufacturing industry priorities.

2.4.1 Annealing

(Papula, Talonen, Todoshchenko & Hänninen, 2014) studied the delayed cracking phenomenon of 300 and 200 series austenitic stainless steels by investigating a method to decrease the risk of delayed cracking by reducing hydrogen content through heat treatments at 673 K (400°C). The study showed that the annealing lowers the concentration of hydrogen content in the stainless steels by 1 to 3 wppm. Hydrogen can severely deteriorate the fracture initiation and propagation resistance of high – strength alloys by facilitating the microscopic processes that constitute fracture initiation and advance. Diffusible hydrogen in the crystal lattice prone to gather in the highly stresses zone of fracture tip, hence, increasing crack propagation (Gangloff, 2003; Wang et al., 2012).

The study showed that annealing the stainless steel before undergoing the drawing process has a distinct effect on the delayed cracking severity as shown in Figure 2.3 (a) and (b), where cups drawn from as-supplied material are compared with cups drawn from

annealed material at 673 K (400°C) for 24 hours (Papula, Talonen, Todoshchenko, Hänninen, et al., 2014).
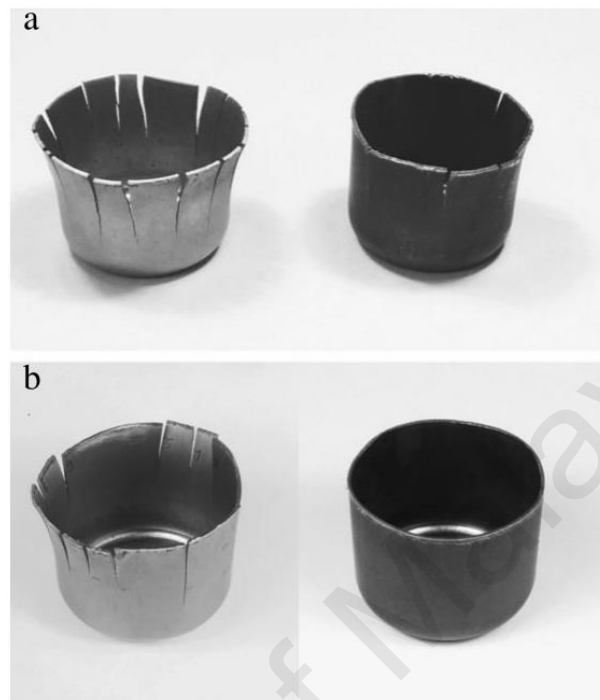
Figure 2.3: Cups of 204Cu (a) and 201 (b) drawn from as-supplied (left) and annealed [673 K (400 C)/24 h, right] blank with LDR 2.0 (Papula, Talonen, Todoshchenko, Hänninen, et al., 2014)

The LDR for delayed cracking is also improved for three different grades of stainless steels. After annealing for 24 hours, the LDR for 204Cu, 201 and 301 improves to 1.6, 2.0 and 2.1 respectively compared to the as supplied LDR of 1.4, 1.7 and 1.8 sequentially. Annealing also slightly reduces the volume fraction of strain-induced α′-martensite created during the drawing process. Through annealing, the reduction of hydrogen increases the stability of austenite. Hence, the volume fraction of strain-induced α′-martensite transformed during the forming process is reduced markedly, eventually minimizing the risk of fracture. In comparison, the difference between the maximum α′-martensite content in the cups drawn from as-supplied and annealed materials is approximately 5 to 7 % at highest (Papula, Talonen, Todoshchenko, Hänninen, et al., 2014).

However, besides the economic disadvantage, annealing is not preferable due to maintaining close tolerances and fine surface quality aspects. Furthermore, the annealing may be useless when high production casting is involved because the cooling rate is seldom as slow or as uniform as it is in the original mold and the process may produce more stresses than the original. Additionally, the annealing process relieves all stresses, leading to product distortion. The facilities of heat treatment are also costly and stress relief cycles are time-consuming (Ragab & Orban, 2000).

2.4.2 Ironing

Many investigators have investigated the effect of minimizing the tool clearance such as ironing employs simultaneously with deep drawing causing a huge reduction in the residual stress and preventing delayed cracks (Siebel & Kotthaus, 1954) (Graber, 1987; Lange & Bruckner, 1990; Yang et al., 1990). Even small ironing strains are sufficient to reduce residual stresses after the deep drawing (Huang & Altstetter, 1991). A simulation using Finite Element Method (FEM) showed that the residual stresses of deep drawn cup after ironing are reduced by 50-65% (Danckert, 1994).

(Ragab & Orban, 2000) investigated a method to reduce residual stress in St1403 and aliminium alloy (AIMg3) deep drawn cups using a set of three ironing dies in addition to a straightening die. The study showed that; subsequent ironing causes a characteristic distribution of the residual stresses along the drawn cylindrical cup wall outer surface. The ironing also causes the tangential stresses to distribute uniformly along the cup wall. Approximately 80% of residual stress reduction obtained through ironing with strains in the order of 0.10-0.20 for St1403 and 0.20-0.25 for aluminium alloy (AIMg3). However, the ironing process requires high accuracy, costly tools and advanced lubrication. In addition, the number of the ironing stages does not affect the residual stresses significantly.

2.4.3 Redrawing process

Delayed cracking in AISI 304 cylindrical cups at limiting draw ratios is also preventable with a 5-stage redrawing process (Huang et al., 2004). Although delayed cracking is observed after a single-stage deep drawing with a limiting draw ratio of 2.15, no cracks are found when the same draw ratio is divided into 5 drawing stages to achieve an accumulated draw ratio similar to the former case. In fact, the accumulated amount of α'-martensite in the 5-stage redrawn cup is larger than in the 1-stage drawn cup for the same draw ratio, yet no crack is found. However, redrawing tools are costlier with greater numbers of drawing stages.

2.4.4 Nickel addition

(Zhang et al., 2012a) studied that the nickel content influences the austenitic stainless-steel susceptibility to internal hydrogen embrittlement. Nickel enhances austenite stability and the stacking fault energy, which causes cross slip, thus, minimizing planar slip participation in fracture to increase the level of ductility (Teus, Shyvanyuk, & Gavriljuk, 2008). According to (Michler, Lee, Gangloff, & Naumann, 2009), add nickel into austenitic stainless steels to prevent the bad effect of hydrogen, the combined consequence of austenite stabilization and promotion of cross slip causes more hydrogen embrittlement resistance and increases macroscopically ductile fracture behavior. However, the application of nickel in Cr-Ni austenitic stainless steels is not effective as nickel tends to segregate, resulting in a heterogeneous microstructure and variation in the distribution of α'-martensite. Additionally, high cost of nickel force stainless steels manufacturers and users to find low-nickel alternatives for conventional nickel containing stainless steel grades (Papula, 2015).

2.4.5 Nano lubricant application

In a typical sheet metal forming operation, a flat blank is plastically deformed to require geometry or shape between a blank holder and die. Hence, the blank is continuously in direct contact with the tool component during the drawing process. It is proven that friction in contact surfaces plays a decisive role in metal forming process (Zareh-Desari, Abaszadeh-Yakhforvazani & Khalilpourazary, 2015) as it determines the sheet deformation and requires amount of punch and blank holder force. Furthermore, friction influences the stresses and strains in the drawn parts material, hence, increasing the quality of the product (El Sherbiny, Zein & Abd-Rabou, 2014). (Simões, 2012) claimed that the success of a cylindrical cup sheet metal forming process is directly linked with the friction coefficient besides drawing speed, BHF, temperature and tools geometry. The assessment of minimizing the effect friction during sheet metal forming process is a very complex task (Figueiredo, Ramalho, Oliveira, & Menezes, 2011).

However, studies have shown that the friction can be easily reduced through the application of a lubricant (Simões, 2012). Lubrication is important to minimize the effect of friction between moving components of metal – forming tools, like the ones used for deep drawing process (Canter, 2009). The inappropriate lubrication during forming operation can cause alarming problems throughout the process like an increase of forming forces, abrasion in die parts, undesirable surface quality and a formation of cracks of sheet material (Yang, 2010).

To improve the tribological properties of lubricants, nanoparticles have been studied as high performance extreme pressure additives (Battez et al., 2007; Bhaumik, Prabhu, & Singh, 2014; Thakre, Thakur, & Tribology, 2015; Zhou, Wu, Zhang, Liu, & Dang, 2001). Due to their Nano size, nanoparticles may be deposited on worn surfaces, hence, reduce friction coefficient, decrease wear debris agglomeration (Mosleh, Atnafu & Belk, 2009;

Rapoport et al., 2003), form tribochemical reaction products at high pressures (Hu et al., 2002) or being tribosintered onto the surface (Battez et al., 2010).

Over the past few decades, extensive efforts by researchers in studying the influence of additives in lubricants have made striking impacts on lubrication application in metal forming operation. (Yoshimura, Torikai, Nishihara, Nonishi, & Inouchi, 2002) recommended an environmentally friendly lubricant additive using wheat flour. They claimed that this material has an extraordinary effect on sheet formability in comparison with conventional lubricants like grease. (Carcel, Palomares, Rodilla & Puig, 2005) studied the application of vegetable oils as lubricant. Through the tests, they observed that this material source is comparable in performance (even without the use of additives) to mineral base oil. (Kosanov, Lenard, Uhrig & Wallfarth, 2006) executed series of flat – die experiments using three types of lubricant oils and two types of additives to ascertain the dependency of friction coefficient to load, lubricant viscosity and relative velocity. The results showed that consistent results can be acquired only by employing lubricant with additive. They also concluded that the friction coefficient reduces with the increasing normal load. (Rao & Xie, 2006) examined the lubrication performance of boric acid along with seven types of conventional lubricants in different metal forming processes. They found that boric acid gives the lowest friction coefficient for sheet metal forming operations. However, liquid and semi-solid lubricants provide well lubrication condition for bulk forming. (Lovell, Higgs, Deshmukh, & Mobley, 2006) scrutinized the combination of canola oil and boric acid as an alternative environmentally friendly lubricant. They reported that the combinational lubricant has high efficiency in minimizing coefficient of friction and optimizing surface finish.

The use of lubricating oils containing nanoparticle additives in various applications has gained an increasing interest in recent years (Khalilpourazary & Meshkat, 2014; Lee et

al., 2009). (Saravanakumar, Prabu, Karthik & Rajamanickam, 2014) employed silver nanoparticles to increase thermal and tribological properties of cutting fluid in turning operation. They reported the material successfully reduces the tool tip temperature, cutting force and workpiece surface roughness.(Mao et al., 2012) utilized water-based Al_2O_3 Nano fluid to grinding process with regard to the minimum quantity lubrication (MQL) approach and the results indicated that Nano fluid MQL can effectively minimize grinding forces and improve workpiece surface roughness. In another research (Lee, Nam, Li & Lee, 2012) employed diamond and Al_2O_3 nanoparticles additives to increase MQL for micro – grinding process and obtained similar results as (Mao et al., 2012).

The effectiveness of lubricants with different nanoparticle additives like CuO, ZnO and ZrO_2 nanoparticles added with polyalphaolefin (Battez et al., 2008), mixture of CuO nanoparticles and coconut oil (Thottackkad, Perikinalil & Kumarapillai, 2012), WS2, MoS2 and hBN nanoparticles dispersed in CIMFLO 20 oil (Mosleh et al., 2009) and CuO, CeO_2 and Al_2O_3 nanoparticles added into SAE 15W40 (Kalakada, Kumarapillai & Perikinalil, 2012) have been investigated in different loading, thermal and contact conditions. The acquired results have confirmed great efficiency of the nanoparticle additives in improvement of tribological characteristics of conventional lubricants. (Battez et al., 2008; Thottackkad et al., 2012) reported that the most suitable tribological performance is often obtainable for a certain amount of nanoparticles concentration.

Previous studies mostly include the application of nanolubricant in cutting and machining operations. Therefore, the remarkable results of this research can be a momentum to investigate the efficiency of nanolubricants in actual sheet metal forming operation like deep drawing as a novel approach. In addition, the effectiveness of nanolubricant in preventing unfavourable defects like delayed cracking will be investigated under elevated BHF.

2.5 Summary

Hydrogen content, microstructure transformation, residual stress and low amount of nickel in stainless steel are the factors caused delayed cracking. Number of methods have been studied to eliminate delayed cracking like annealing, ironing, redrawing and nickel addition. Regardless of the effectiveness of these methods in preventing fracture, there are few drawbacks which require other alternatives to effectively control the occurrence of delayed cracking in deep drawn stainless steel product. Number of studies have highlighted the application of Nano lubricant in metal forming operation to eliminate unnecessary defects. Therefore, this study will investigate the effectiveness of Nano lubricant under elevated BHF in preventing delayed cracking.

CHAPTER 3: METHODOLOGY

3.1 Introduction

The goal of this chapter is to present details regarding the experimental and numerical procedures involved in this research; the details of experimental procedures using deep drawing operation, material properties and preparation like nanolubricant, research parameters and the procedures of data collection and analysis using particular advanced machines. The overall research methodology is illustrated in Figure 3.1.

```
                    ┌──────────────┐
                    │    START     │
                    └──────┬───────┘
                           ↓
                    ┌──────────────┐
                    │  Literature  │
                    └──────┬───────┘
                           ↓
                 ┌────────────────────┐
                 │ Design of experimental │
                 │      apparatus     │
                 └──────────┬─────────┘
                            ↓
          ┌────────────────────────────────────┐
          │ Planning of experimental conditions, │
          │ schedule, details of experimental and flow. │
          └──────────────────┬─────────────────┘
                             ↓
                    ┌──────────────────┐
                    │ Procurement of   │
                    │ hardware and materials. │
                    └────────┬─────────┘
                             ↓
                    ┌──────────────────┐
                    │ Practice conducting │
                    │ deep drawing machine. │
                    └────────┬─────────┘
                             ↓
   ┌──────────────────────────────────────────────────────┐
   │ Experiment execution of deep drawing using stainless steel sheet │
   │ under elevated blank holding force with the aid of Nano lubricant. │
   └──────────────────────────┬───────────────────────────┘
                              ↓
                        ◇─────────◇              ┌──────────────┐
                       │  Check   │──────────────│ Improvement  │
                        ◇────┬────◇              │  measures    │
                             ↓                   └──────────────┘
                    ┌──────────────────┐   ┌──────────────┐
                    │ Analysis of result │───│ Journal paper │
                    └────────┬─────────┘   └──────────────┘
                             ↓
                       ┌──────────┐
                       │   END    │
                       └──────────┘
```
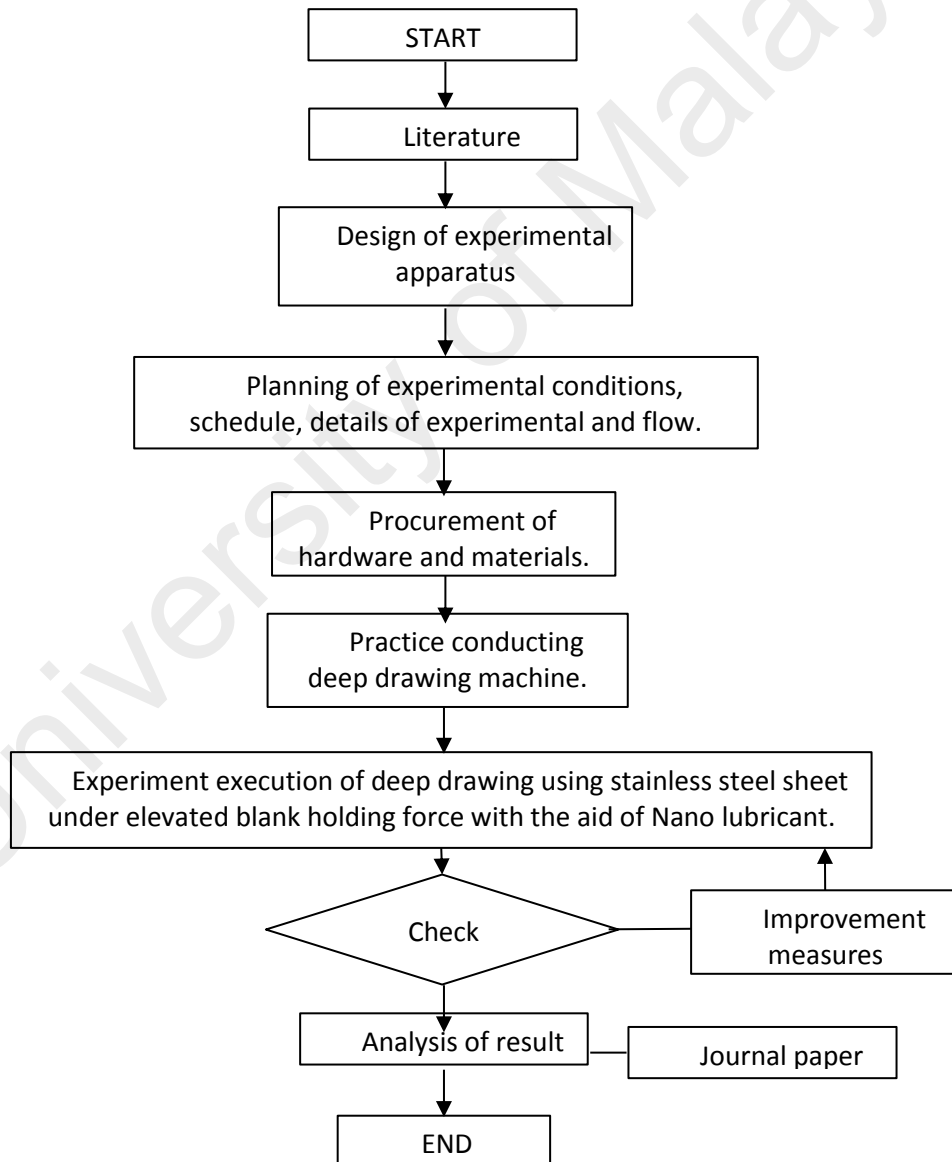
Figure 3.1: Methodology flow chart

3.2 Experimental procedure

3.2.1 Test material and cup testing

The studied material was a metastable austenitic stainless steel SUS304. The 1.2 mm thickness material was presented in the form of cold-rolled sheets of 500 mm x 500 mm in an annealed final state before undergoing a cutting process into circular blanks of 72 mm in diameter using laser –cut machine. The mechanical properties of the blank are shown in Table 3.1. The chemical composition of the test material measured by the supplier is given in Table 3.2. The chromium and nickel contents were 18.3 wt% and 8.07wt%, respectively. The nickel content of a sheet was less than 11%, hence, it was susceptible to delayed cracking. Despite the high tensile strength, the total elongation of SUS304 at 600 MPa and 52% respectively.

Table 3.1: Mechanical properties of SUS304 (Mill certificate from maker, POSCO)

Mechanical properties	Value
Tensile strength, MPa	600
Yield strength, MPa	262
Elongation, %	52
Hardness, HV	180

Table 3.2: Chemical composition of SUS304 austenitic stainless steel, wt% (Mill certificate from maker, POSCO)

Element	Cr	Ni	C	Mn	Si	Mo
Composition	18.3	9.2	0.04	1.5	0.5	0.18

The experimental set up and its diagram of deep drawing test are shown in Figure 3.2. The deep drawing tests were conducted at room temperature using a 25-ton shop press. A 30-ton load cell was placed between the press and the punch to obtain the load data during the drawing process. A laser distance sensor was positioned right above the press

plate. The press plate moved along with the punch during the test and the laser sensor captured the travel distance data. Both the load and distance signals were recorded with a data logger at a sampling rate of 10 Hz. A punch holder having a tight mating tolerance with the punch was inserted in the center of the blank holder to obtain the central alignment of the punch during the drawing process for poor central punch alignment causes uneven cup height.
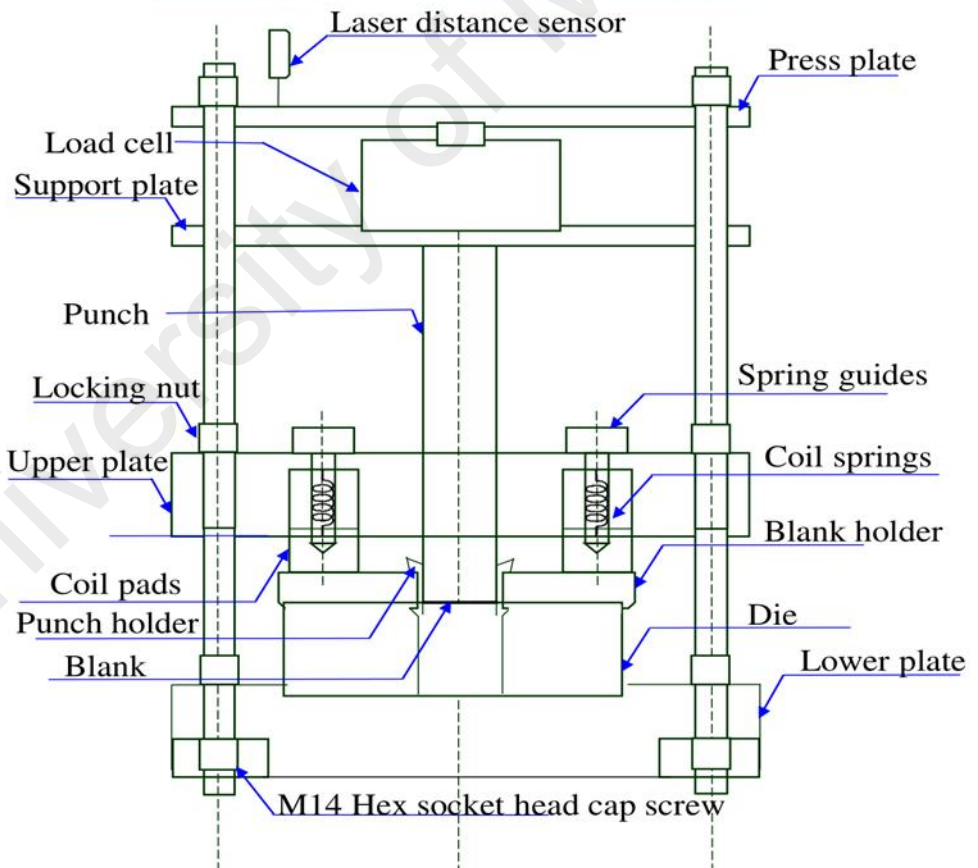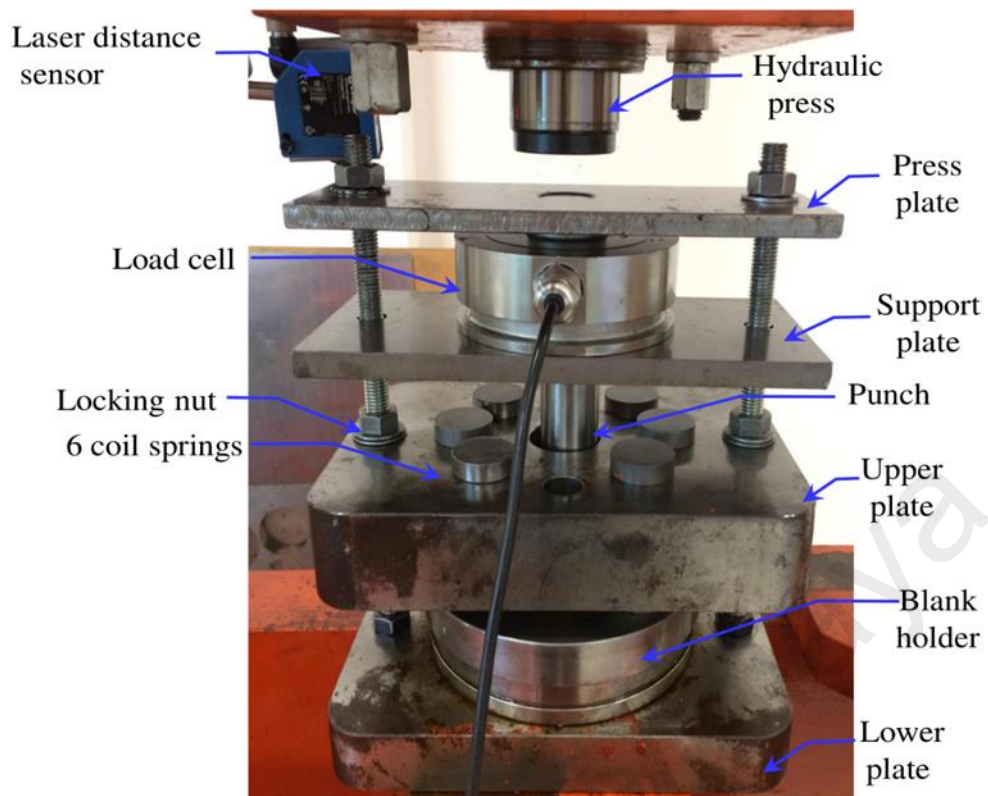
Figure 3.2: Experimental set up

3.2.2 Generating constant BHF with coil springs

Prior to the deep drawing test, it was necessary to set a high and constant BHF. To do so, the punch was removed and a 10-ton load cell was placed between the upper plate and the press plate to measure the target BHF. The press compressed the coil springs located inside the upper plate to a target value. All coils had a spring constant of 0.75 kN/mm with a maximum deflection of 8 mm. The number of coils used could be increased to correspond to the target BHF values. A maximum of eight coils may be used with this setup, which is capable of generating BHF up to 48 kN. The coils were arranged symmetrically to obtain a balanced holding force toward the blank. Coil return was prevented by slightly tightening the locking nuts above the upper plate without increasing the target BHF. After releasing the press, the two nuts maintained the target BHF. The 10-ton load cell was then removed and replaced with the punch and 30-ton load cell for the drawing test using the same setup.

3.3 Detailed experimental conditions

Figure 3.3 shows the details of the experimental conditions for the deep drawing test. Laser-cut circular SUS304 blanks measuring 72 mm in diameter with an initial sheet thickness of 1.1 mm were used in the experiment. The cutting edges around the blanks were grinded finely using a grinding machine to eliminate the hard oxide layers and sharp edges resulting from the laser cut.

Before the drawing process, the tools geometry and surface were ensured to be in a good condition as the state could influence the amount of friction induced and final part appearance. The limit drawing ratio (LDR) and the residual stress are greatly related with the tools geometry, particularly the die and punch shoulder radius (Özek & Bal, 2009).The tools should not damage, mark or weaken the final part.

Firstly, the forming die and blank holder were cleaned using ethanol to remove the corrosion protective oil layers. The tools were then being polished to mirror finish using Micro-Mesh sand paper ranging from 400 to 2000 grid to eliminate scratches and wear. After the sand paper polishing process, the tools were polished using diamond paste (average size of 3 µm) to obtain a finer surface finish. Finally, the tools were cleaned using ethanol to remove the dirt or unattended oil during previous polishing process in order to obtain a fine lubricated contact when the blank being sandwiched between the die and blank holder, specifically in the flange region. After the drawing operation, drawn part as well as punch and blank holder were cleaned to remove the Nano lubricant oil layers and then applied with corrosion protective oil.

The diameters of the punch (D_p) and die (D_d) were fixed at 34 and 37.4 mm, respectively. An uncoated and hardened drawing die made of tool steel was used in the test. Tool and carbon steels were commonly used as the die and punch material. However, tool steel was preferable for heavy duty tasks due to its harder property than carbon steels. A commercial lubricant containing 1, 2 and 3 wt% SiO_2 was applied to the die and blank holder surfaces only, including the die corner to reduce the friction. The punch and blank were kept dry.

The BHF value was gradually increased after each successful drawing until the delayed cracks disappeared and reappeared. The crack-free ranges for each SiO_2 concentration were determined. The successful drawn cups were observed every 1 hour to determine the time for the first crack to form. The number of cracks was also recorded. To prevent results scattering, each condition was repeated twice. An additional test was performed if the first two results were conflicting. Prior to the drawing test, the limiting draw ratio (LDR) was determined using the following formula(Bandyopadhyay et al., 2016):

$$LDR = \frac{D_b}{D_p} \qquad\qquad Eq.\,3.1$$

Where LDR is limited drawing ratio, D_b is blank diameter and D_p is punch diameter. Hence, the LDR for the blank to be successfully drawn without cracking was 2.12. The draw ratio in the test was maintained at 2.12 because the blank's susceptibility to delayed cracking was the highest if exceeding this LDR. The appearance of cracks in the cups after the drawing process was examined visually.
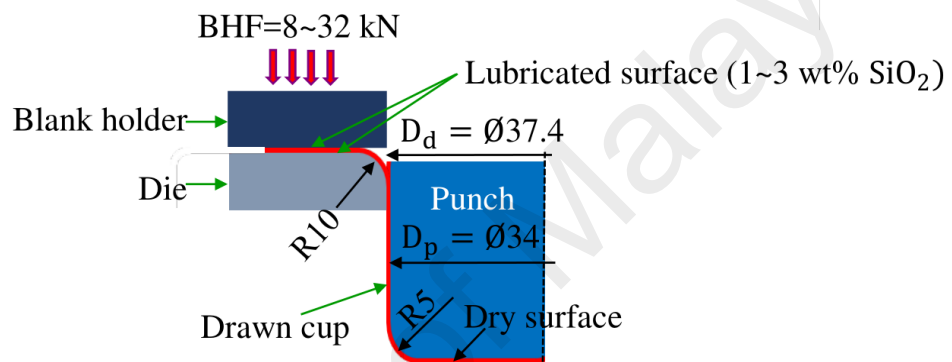

Figure 3.3: Detailed conditions for deep drawing test

Table 3.3: Experimental conditions

Fixed Conditions	
Nano powder material	Silicon Oxide, SiO_2
Lubricant type	ACI PRESSCUT J133
Blank material	SUS304
Blank diameter, mm	72
Blank initial sheet thickness, mm	1.1
Limited drawing ratio, LDR	2.12
Punch diameter, mm	34
Die diameter, mm	37.4
Variable Condition	
Nanolubricant concentration, wt%	1,2 and 3
BHF	8~31kN

3.4 Nano lubricant preparation

A commercial deep drawing lubricant (ACI PRESSCUT J133) with viscosity of 285 cSt at 40^OC containing a corrosive inhibitor and extreme pressure additives was added to three beakers containing 1, 2 and 3% SiO_2 nanoparticles, giving difference weight percentage of concentration as shown in Table 3.4. The hardness of the spherical nanoparticles was 1000 Hv, which was approximately 5.6 times greater than the blank with an average size of 5 ~ 15 nm. The mixture of lubricant and nanoparticles was stirred well with a magnetic stirrer for at least 20 minutes.

$$SiO_2 \text{ Mass}, \% = \frac{\text{Mass of } SiO_2, \text{ g}}{\text{Mass of lubricant, g}} x100 \qquad Eq. 3.2$$

$$\text{Concentration, wt\%} = \frac{\text{Mass of } SiO_2, \text{g}}{\text{Total mass of the solution, g}} x100 \qquad Eq. 3.3$$

Table 3.4: Mixture ratio of SiO_2 lubricants

SiO_2 Mass, g	Lubricant, ml(g)	SiO_2 Mass, %	Concentration, wt.%
2.5	250	1	0.990
5.0		2	1.961
7.5		3	2.913

Nanomaterials like SiO_2 nanoparticles tend to be agglomerated when mixed into oil. Deagglomerating and dispersing are highly necessary to control the bonding forces after wettening the powder. The ultrasonic breakup of the agglomerate structures in aqueous and non-aqueous suspensions allows utilizing the full potential of nano size materials. Therefore, beakers were placed in an ultrasonic cleaning bath machine (ultrasonic power of 50 W and frequency of 42 kHz) for 8 hours to ensure the particles dispersed uniformly in the oil.

According to (Tan, Abe, Daodon, Takahashi, Mori, & Purbolaksono, 2016), 6-hour ultrasonication process is sufficient to ensure the particles dispersed uniformly in the oil. In this study, the mixtures were vibrated for 8 hours. However, there is a tendency for SiO2 nanoparticles to agglomerate. Therefore, the well-dispersed nanolubricant was immediately applied to the target surfaces in the test after ultrasonication to avoid nanoparticle condensation.

3.5 XRD analysis

A quantitative assessment of austenite,ε- andα′-martensite phases along the cup wall was done at the specimen surface and through the thickness by Empyrean Panalytical XRD using copper (Cu) radiation. The diffraction angles (2θ deg) used were from 30° to 80°. The diffraction peak for each phase was generated by specific parallel atomic planes in the crystal. The diffraction peak positions contain information about the length d_{hkl} between those atomic planes. In this study, the integrated intensities of the austenite (111), (200) and (220), ε-martensite (110) and α′-martensite (211) diffraction peaks were measured to obtain the volume concentration percentages of FCC, HCP and BCC in steel.

3.6 Residual stress measurement

3.6.1 X-ray diffraction

The residual stress of non-cracked cups was examined on 4 different points with different heights of 30 ,60,80 and 100% from cup bottom using the classical $\sin^2\Psi$ (multi-angle) method (Bragg's law) with an X-ray diffractometer AutoMATE II as shown in Figure 3.5.
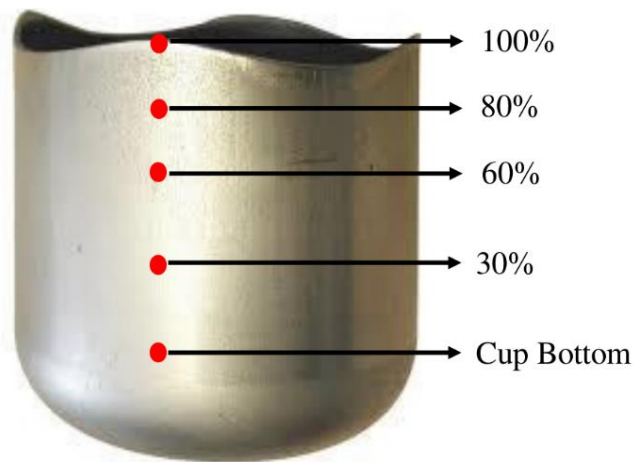
Figure 3.4: Cups divided and marked into 4 different heights from bottom for XRD analysis

The shift in diffraction peak position (2θ angle) was recorded as a function of the sample tilt angle Ψ. The tilt angles used in the measurements were 0°, 5°, 15°, 30° and 45°. The measurements were accomplished by employing Cr-Kα radiation. The middle peak positions were defined with the peak fit (Pearson VII) method. The strain values evaluated were converted into stresses using Hooke's law, assuming linear elastic and isotropic material characteristics.

Figure 3.5: X-ray diffractometer AutoMATE II

3.6.2 Ring slitting method

A cheap and easy separation technique called as split-ring test was developed to estimate the residual stresses along the side wall of deep drawn cups (Hong et al., 2014). The cup's residual stresses in this study were estimated using the same method based on residual stress relaxation. The full deep drawn cups were sectioned into 4 rings in different heights of 30, 60, 80 and 100% from cup bottom using electrical discharge machining (EDM). The rings were then slit in the longitudinal direction along a radial plane with EDM to obtain an opening gap. The ring opening and diameter differences before and after slitting were measured and calculated. The difference between the ring diameters, before and after slitting, provides a direct measure of the delayed crack phenomenon, and indirectly, of the residual stress amount induced in the formed cup (Demeri, Lou, & Saran, 2000).The residual stresses were then computed using equation 3.6 (Jung et al., 2017), where E is modulus of elasticity (200 GPa), t is cylindrical cup wall thickness, D_O is ring diameter before slitting, d is ring opening distance and s is EDM wire thickness

$$\sigma = E.t\left(\frac{1}{D_O} - \frac{1}{D_O + \frac{d-s}{\pi}}\right) \qquad Eq.\,3.4$$
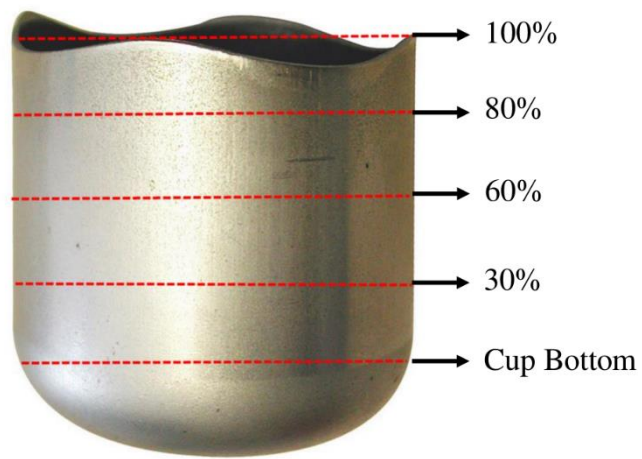

Figure 3.6: Electrical Discharge Machining (EDM)

Figure 3.7: Before: Cups divided into 5 parts in different heights

Figure 3.8: After: Slit cylindrical drawn cup into 5 different heights

CHAPTER 4: EXPERIMENTAL RESULT AND DISCUSSION

4.1 Drawing test

Large test series of deep drawing cup tests were conducted using a 25-ton shop press. Too low BHF allows the blank sheet wrinkling (Afshin, Kadkhodayan, & Design, 2015). Hence, series of preliminary tests were carried out starting with the lowest BHF of 4 kN and gradually increased to determine the minimum ideal BHF giving a well-formed cylindrical cup without wrinkling.1~ 3 kN were ignored due to too low compression force. From the pretests, wrinkled blanks were observed when subjected to 4 to 7 kN of BHF. Therefore, the cups were first drawn under 8 kN of BHF, giving a well-formed cylindrical cup before gradually increased after each successful drawing until the delayed cracks disappeared and reappeared. Table 4.1 shows the SUS304 drawn cylindrical cups in the experiments after undergo an incubation period under different BHFs with nanolubricants containing $1 \sim 3$ wt% SiO_2 concentrations at the limiting drawing ratio of 2.12.

Figure 4.1: Wrinkling cup

Table 4.1: SUS304 drawn cylindrical cups for different BHFs and SiO₂ concentrations

Concen-tration (wt%)	Drawing results BHF (kN) {X:Cracked} OR {O:Okay}			
1	27{X}	28 {O}	29 {X}	
2	8 {X}	15 {X}	25 {X}	28 {X}
	29 {O}	30 {O}	31 {O}	32{X}
3	27{X}	28 {O}	29 {O}	30 {X}

The widest BHF range without cracking was determined for 2 wt% from 29 ~ 31 kN, followed by 28 ~ 29 kN for 3 wt% and 28 kN for 1 wt%. Delayed cracks were observed below and beyond this BHF range. The cracks initiated at the upper cylindrical cup edge and developed linearly in the depth direction towards the bottom. The fractures in the drawn cups were successfully eliminated by applying approximately 3.6~3.9 times the minimum ideal blank holding force with the aid of nanolubrication during the drawing operation.

Overall, the increase in SiO_2 concentration scarcely reduced the minimum BHF needed to prevent the fractures. To observe the influence of nanolubrication in preventing delayed cracks, same procedures were conducted using similar lubricant containing 0 wt% SiO2 within the same BHF range i.e. from 8 kN to 32 kN. The results show that, delayed cracks were observed in these cups for all BHF, thus, the application of nanolubrication in the deep drawing tests contributed to the prevention of delayed cracks.

The crack reformation was due to the worsened nanolubricant tribological performance when undergoing excessive pressure allowing high friction induction. In deep drawing process, friction plays a vital role as it determines the sheet deformation and requires amount of punch and blank holder force. Furthermore, friction influences the stresses and strains in the drawn parts material, hence, increasing the quality of the product (El Sherbiny et al., 2014). (Simões, 2012) concluded that, the success of a cylindrical cup sheet metal forming operation is directly dependent on the friction coefficient besides punch speed, blank holder force and tools geometry.

In general, the nanoparticles like SiO_2 used in this research were utilized as a filler of contact surfaces valleys (mending effect) or operate as a ball bearing during sliding which to prevent contact between the metal surfaces, hence, reducing the friction when certain amount of force was exerted. The addition of nanoparticles in lubricating oil presented

four significant effects (A) ball bearing effect between the contacting surfaces (Chinas-Castillo & Spikes, 2003; Lee et al., 2009; Rapoport et al., 2002; Wu & Kao, 2011) (B) protective film to mitigate friction and coating the rough surface (Ginzburg et al., 2002; Hu et al., 2002; Rastogi, Yadav, & Bhattacharya, 2002; Xiaodong, Xun, Huaqiang, & Zhengshui, 2007), (C) mending effect where the Nano lubricant fulfill the friction crack or asperities due to loss of mass (Lee et al., 2009; Liu et al., 2004) and (D) polishing effect where the friction surface is diminished by abrasion assisted nanoparticles (K. Lee et al., 2009; Tao, Jiazheng, & Kang, 1996). Combination of these effects has led to significant enhancement of extreme pressure limits and load carrying capacity of base lubricants. The role of nanoparticles in the friction surface is presented in Figure 4.2.
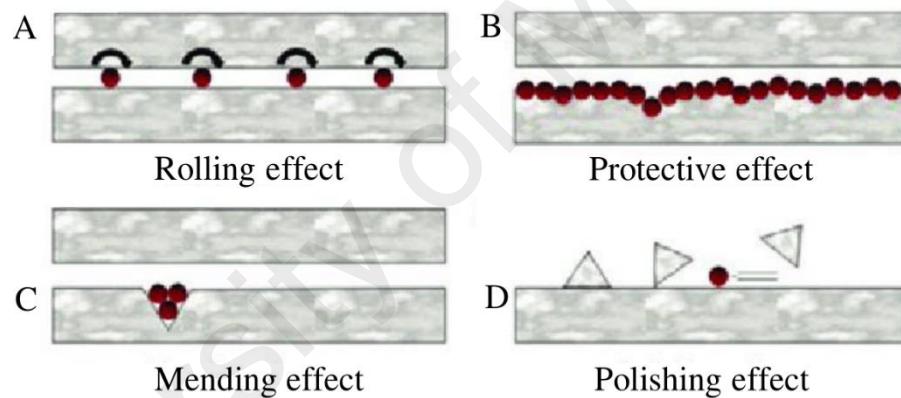
Figure 4.2: Role of nanoparticles in the lubricating oil (K. Lee et al., 2009)

However, this special effects of nanoparticles tend to decrease under high extreme pressure, eventually, lowering the friction resistance which result in delayed cracking (Thirumalaikumaran, 2017). From the results, the fracture reappears after exceeded non-crack BHF range shows that the maximum load-carrying capacity has been achieved and the tribological performance of the nanolubricant is totally deteriorating. There are a number of parameters influencing the friction like the amount of applied load, lubricant viscosity and surface roughness of the tooling (Başpınar & Akkök, 2016). Under heavy load condition, the nanolubricant becomes more stressed and its capability in reducing friction prone to lessen especially under metal-to-metal interactions (Choi et al., 2011).

At high pressure, the nanoparticles tend to crush during the sliding or ploughing through the base metal in case of harder nanoparticles (Thakre et al., 2015). In this study, the hardness of the SiO_2 spherical nanoparticles was 1000 HV, which was approximately 5.6 times greater than the blank. The crushed nanoparticles tend to agglomerate, eventually, causing plough marks on the material, hence, generating more friction force (G. Zhang, Chang & Schlarb, 2009). The crushed nanoparticles significantly diminish the ball bearing effects during sliding and protective film between the contact surfaces as they get thinner (Battez et al., 2007) as in this experiment, the blank holder and die surfaces would have a direct contact with the circular blank , hence, allowing high induction of friction force resulting in fracture. In addition, under high pressures, the lubricant film thickness becomes thinner, thus Mixed Lubrication (ML) or Boundary Lubrication (BL) occur with nanoparticles separating contacting surfaces. This causes more asperities to contact and leads to a higher coefficient of friction (Başpınar & Akkök, 2016).

On the other hand, under excessive pressure, the nanoparticles tend to flow out of the contact region upon shearing, hence, the shearing surfaces do not earn any tribological advantages from the nanoparticles (Akbulut, 2012). In other words, it is vital for the nanolubricant to stay in the contact zone to protect shearing surfaces when certain force is exerted during drawing process.

During the experiment execution, a question arose whether the amount of lubricant applied on the die and blank holder was important or not because it tended to flow out of the contact areas. (Simões, 2012) concluded that the amount of lubricant does not have a relevant influence in friction induction during drawing process by considering three different amounts of lubricant, i.e. 8.4, 20.2 and 45.7 g/m^2 under constant BHF. Through the punch force evolution - displacement curves and drawn cup's wall thickness distribution analysis, the lubricant amount influence was negligible as the forming force

against displacement and cup wall thickness distribution for all three variables were very close (Simões, 2012). Even though the amount of lubricant seems to have a negligible effect in the drawing conditions, it is vital to consider the effective application of lubricant in the tools contact surface as a basic to acquire a successful product.

From this standpoint, the nanoparticle size can overcome this problem as the asperities of shearing surfaces can act as physical barriers that keep nanoparticles within the contact regions, the average size of SiO_2 nanoparticles used was 5 ~ 15 nm. (Akbulut, 2012) concluded that size of the nanoparticles is one of the most critical parameters influencing the tribological properties of Nano lubrication beside shape, nanostructure and concentration of the nanoparticles.

When the characteristic roughness length scale of shearing surfaces is smaller than the nanoparticles radius, the ratio of roughness to the nanoparticles radius is an indicator of how much lateral force is needed to displace a nanoparticle out of an asperity barrier as shown in Figure 4.3. In other words, if the nanoparticles are too large and non-adhering, they tend to escape from the contact region, resulting in poor lubrication effect. However, if the roughness length scales are larger than the nanoparticles radius, the valleys between asperities of the shearing surfaces can be filled with nanoparticles, hence, increasing the tribological properties.
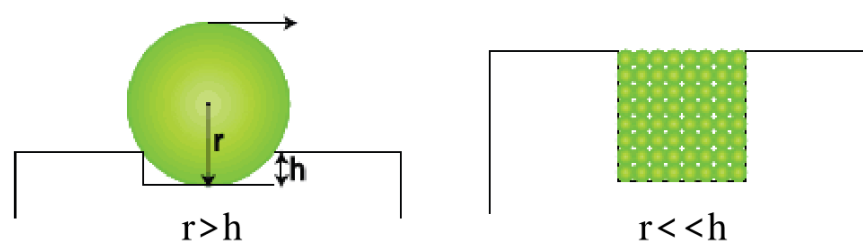

Figure 4.3: The effect of surface roughness of nanoparticles between the shearing surfaces asperities (Akbulut, 2012)

A number of cracks in all deep drawn cups, together with the time taken for the first crack to form with different concentrations of SiO_2 and BHFs are summarized in Table 4.2 and presented in Figure 4.4. To refine and verify the results, the tests were repeated twice. The shortest incubation time taken for the first crack to form after the deep drawing operation varied from 1 hour to 5 days. Samples 1 and 2 exhibited the similar tendency for each condition, hence, testing the 3rd sample was neglected.

The pattern shows that, the increment of BHF gave significant effects on the duration for the first crack to appear when a longer time needed i.e. from 2 hours at BHF of 8 kN to 5 days at BHF of 28 kN with 2wt% SiO_2. In addition, the duration decreased from the maximum non-crack BHF of 31 kN to 4 hours at BHF of 32 kN due to the deteriorated function of nanolubricant tribological performance under high pressure when its limit was exceeded. As assumed above, there are 2 possible factors contributing to poor lubricant tribological performance when subjected to high pressure; first under high extreme pressure, the nanolubricant becomes more stressed and its capability in minimizing friction prone to lessen as the nanoparticles tend to crush during sliding. Hence, the four nanoparticles special effects; (A) ball bearing effect between the contacting surfaces (Chinas-Castillo & Spikes, 2003; Lee et al., 2009; Rapoport et al., 2002; Wu et al., 2011) (B) protective film to mitigate friction and coating the rough surface (Ginzburg et al., 2002; Hu et al., 2002; Rastogi et al., 2002; Xiaodong et al., 2007), (C) mending effect where the nanolubricant fulfill the friction crack or asperities due to loss of mass (Lee et al., 2009; Liu et al., 2004) and (D) polishing effect where the friction surface is diminished by abrasion assisted nanoparticles be likely to deteriorate. Second the nanoparticles tend to flow out of the contact region upon shearing under excessive pressure, hence, no benefits in tribological properties resulting in delayed cracking occurrence.

Table 4.2 shows the number of cracks for 1~3 wt% SiO_2 under elevated BHFs. Overall, the number of cracks increased as the BHFs increased from 27 to 30 kN for 1 and 3 wt% SiO_2 from 4 to 7 and 4 to 6 respectively. However, different trend was observed for 2 wt% SiO_2 as the number of cracks increased gradually from 2 to 4 when the BHF was increased from 8 to 28 kN before dropping to its original value from no crack at BHF of 31 kN to 2 under largest BHF of 32 kN. In comparison, the number of cracks for 2 wt% SiO_2 was smaller than for 1 and 3 wt% under the same BHF range (27 – 32 kN).

Meanwhile, different trend was analysed for the duration for first crack to form as shorter time is required when the BHF was increased for 1 and 3 wt% SiO_2 from 1 to 1 and 3 to 1 hour respectively. However, the trend was different for 2 wt% SiO_2 as longer time required to form the first crack when the BHF was increased from 8 to 28 kN from 1 hour to 5 days before decreasing markedly to 4 hours after exiting crack-free range under excessive BHF of 32 kN. The both trends of number of cracks and duration for appearance of first crack prove that the increase in SiO_2 concentration was hardly to influence the minimum amount of BHF required to prevent the delayed cracks.

Table 4.2: Number and time taken for appearance of first crack for different concentrations SiO₂ of under different BHFs

Table 4.2: Number and time taken for appearance of first crack for different concentrations SiO_2 of under different BHFs

SiO_2 (wt%)	BHF (kN)	No. of cracks	Duration for first crack
1	27	4	1 h
	28	-	No crack
	29	7	1 h
2	8	2	2 h
	15	2	2.5 h
	25	3	3 days
	28	4	5 days
	29	-	No crack
	30	-	No crack
	31	-	No crack
	32	2	4 h
3	27	4	3 h
	28	-	No crack
	29	-	No crack
	30	6	1 h
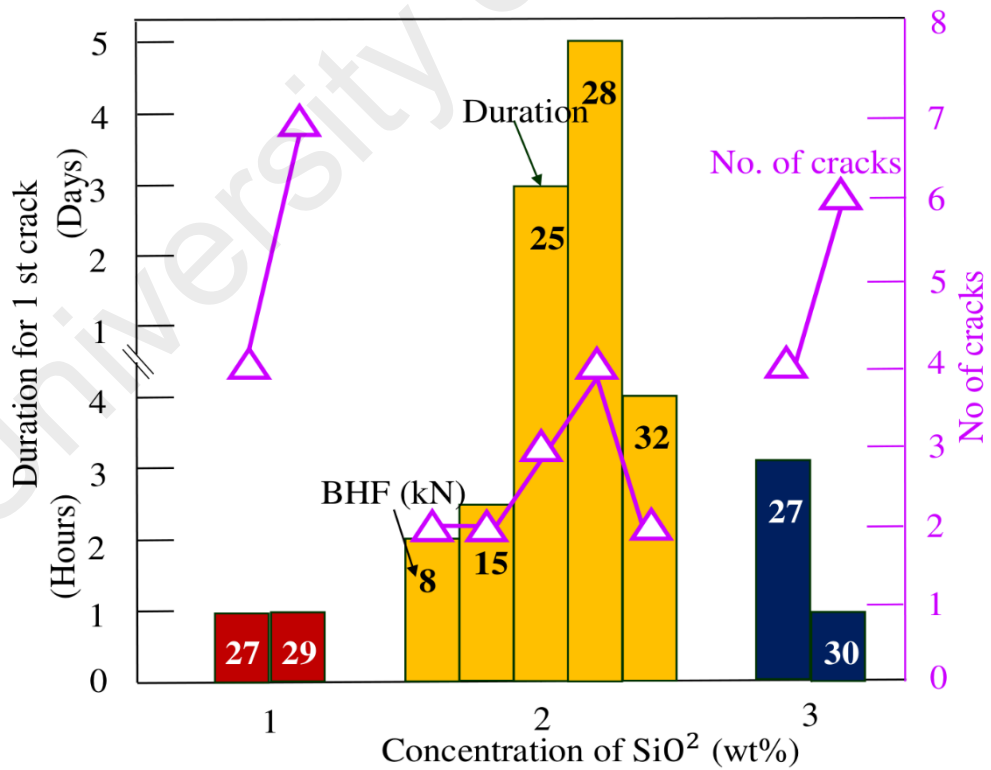
Figure 4.4: Comparison of number and time taken for first appearance of cracks

4.2 Cups wall thickness

Figure 4.5 displays the change in cup wall thickness under different BHFs for 2 wt% SiO_2 measured from the central region to the flange of the cups. It is clearly shown that the trend of cup's wall thickness distribution was similar when subjected to 8 to 31 kN of BHF.
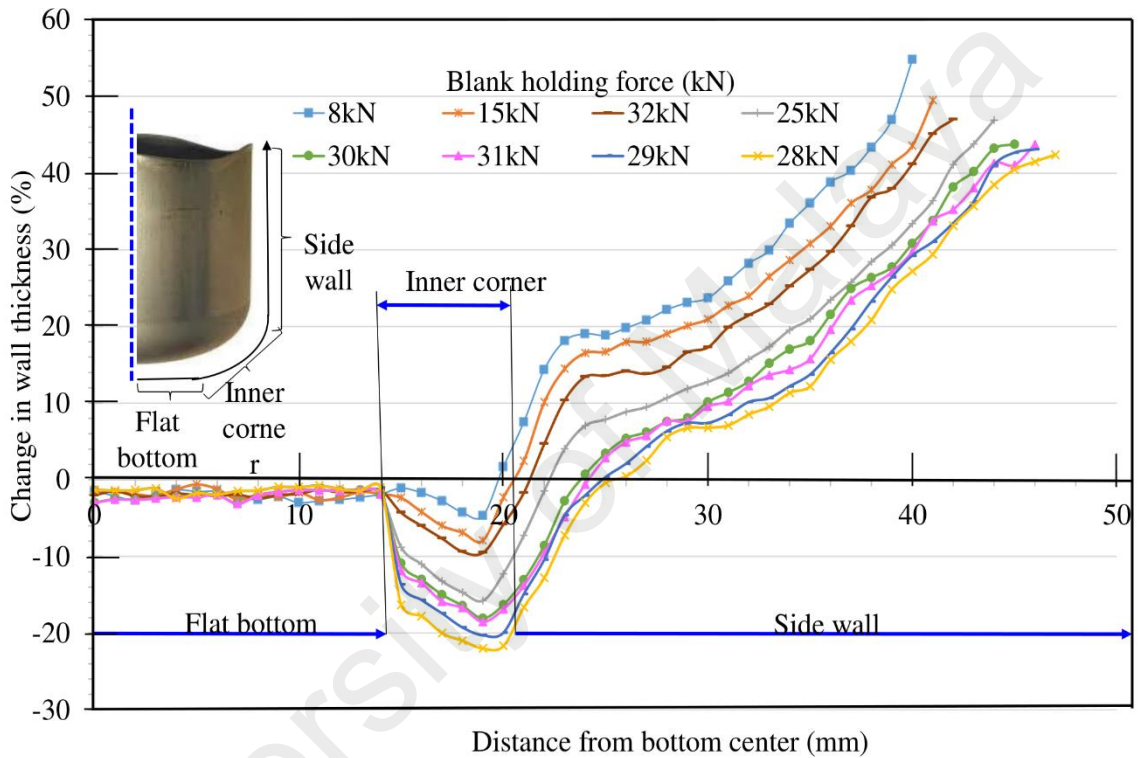
Figure 4.5: Change in wall thickness of cups under different BHFs for 2 wt% of SiO_2
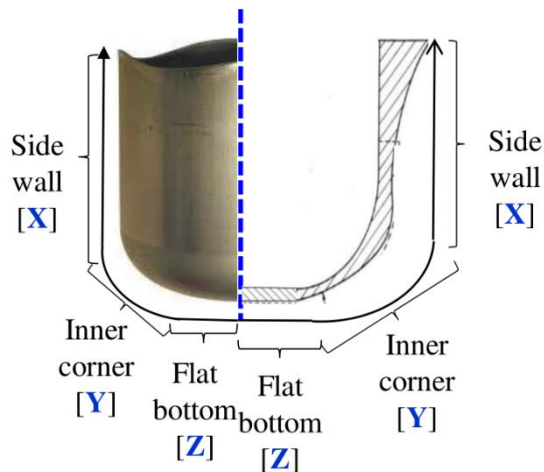
Figure 4.6: Cup wall thickness in three separated regions

Figure 4.6 shows the wall thickness distribution around the cups' inner corner and side wall. The drawn cup is divided into three regions X, Y, and Z. The outer annual region X is compressed between the circular blank holder at its top area and the die at its bottom area as shown in Figure 4.7. When the punch is moving downwards and rammed the blank, the material in region X begins to move progressively inward towards the die profile under the effect of the subjected tensile stress. The action implies the radii in this region to be decreased, hence induced compressive hoop stress resulting to the increment in the material thickness at the outer part of region X.

The thinning occurs by plastic bending under the influence of the tensile stress when the material in region X passes over the die profile. The thinning formed at this outer region increase the material thickness, particularly at inner corner region. The critical strain where the material is thinnest is observed at region Y because it is subjected to bending and sliding over the die profile, stretching between the punch and die in the clearance zone and also sliding and bending over the punch profile.

The last finding is that the bottom wall of region Z is not affected by the drawing operation when the thickness is remains without change because this region is subjected only to stretching and sliding over the punch head. When the punch is moving downwards the forming pressure will be initially applied on the blank surface underneath the punch head. Since the friction coefficient punch surface is high, hence the frictional forces generated at this zone will overcome any possible sliding resulting to non-increment of tensile force at the cup bottom. Therefore, the wall thickness remains with no significant thinning occurs.

Overall the wall thickness around the cups' inner corner and side wall under different BHFs for 2wt% SiO_2 decreased constantly when the amount of BHF increased gradually from 8 to 31 kN due to the rising BHF (Zaid, 2016) during the drawing process. (Simões,

2012) concludes that, the success of a cylindrical cup sheet metal forming operation is directly depended with the amount of blank holder force (BHF) applied. The reason behind this behaviour could be described by the fact that the rising in BHF leads to an increasing in tensile stress in the cup's wall side. Number of studies concluded that tensile residual stress induces environmentally assisted cracking initiation, leading in greater risk of damage (Hashmi, 2014; Nedoseka, 2012; Todinov, 2006; Ye, 2015). Once the punch moved downwards and rammed the blank the material in flange region starts to move progressively inwards towards the die profile under the effects of the induced tensile stress. Hence, the greater the load applied the larger tensile stress generates in the material resulting to more material elongation in the axis of the applied load. However, a too high BHF drives to high tensile strains that causes high materials elongation eventually cause necking, but a too low BHF allows the blank sheet wrinkling. Hence, it is of paramount concern to determine the appropriate value for the blank holding force.

Additionally, the increasing in BHF also caused high stretching force, hence influences the cup's thickness distribution. Figure 4.7 shows the significant contact regions of a cylindrical cup where stretching takes place when undergo deep drawing operation identified by (Schey, 1983). 1 and 2 regions are known as flange region. The first region is placed between the blank holder and the blank, and the second is between the circular die and the blank. The third region characterized the contact between the die radius and the blank where the nominal pressure here is approximately ten times larger than flange region. The tension force is high and stretching play an important role in this region. The contact between the punch flank and the blank occurs in forth region where the blank is stretched, although no real contact occurs. The fifth region corresponds to the contact between the punch radius and the blank where the tension force reaches high values. The sixth region characterizes the contact between the bottom of the punch and the blank. At this point, the blank is mainly subjected to stretching (Schey, 1983).
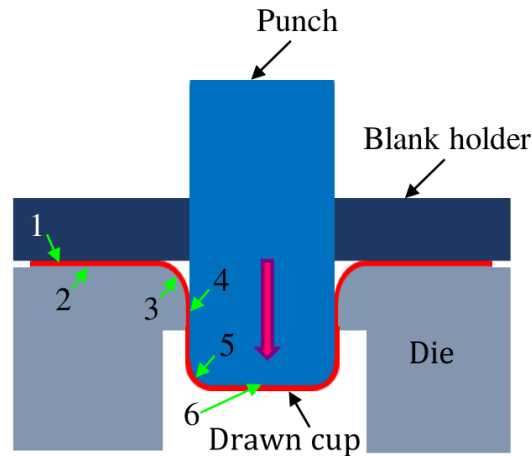
Figure 4.7: Significant contact regions of a cylindrical cup where stretching takes place when undergo deep drawing operation

During the drawing test, the blank was compressed between the circular blank holder and the die as shown in region 1. When a force was exerted moderately, the material in region 1 was allowed to flow inwards towards the die cavity. However, when a larger force was applied on the blank holder, the material was not allowed to flow from the flange area towards the die cavity , and the process was stretched which resulted in the material movement, that influenced the thickness distribution (Sniekers, 1996). Therefore, the higher the BHF applied the more stretching takes place, resulting in thickness reduction. To ensure the blank followed the punch movement through the die, the friction in region 5 must be sufficiently high. However, the extreme level of stretching caused by high BHF can cause necking and tearing in region 5 due to an excessive reduction of material thickness as observed when the BHF was extended to 33 kN as shown in Figure 4.8.
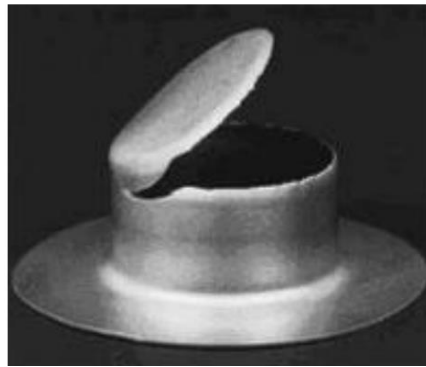
Figure 4.8: Necking cup was observed after subjected to 33 kN

Approximately, 20% maximum decrease in wall thickness was obtained along the side walls of the drawn cups when the BHF was raised from the ordinary value of 8 kN to 28 kN. Once entering the free-crack range from 29 to 31 kN, the amount slightly rebounded before rebounding significantly beyond this range at BHF of 32 kN, resulting in crack reappearance.

The rebound was due to the restricted deformation in the flange portion resulting in the slightly increase in frictional force. A study claims that the flow of metal into the die cavity affects the quality of deep drawn components. Excessive flow may result in wrinkles within the part, while an insufficient flow can lead in fracture (Reddy, 2012). In metal forming operation, friction between workpiece and tool is an imperative parameter influencing the material flow and strain distribution where in deep drawing the main source of friction is in the blank holder (Başpınar & Akkök, 2016) when the flange region of the blank being clamped between blank holder and circular die. Thus, the formability of metallic blank sheet relies on the friction at the tooling interface in addition to its material properties (Wilson, Hsu, & Huang, 1995).

In addition, limited drawing ratio (LDR) is one of the most vital parameters in deep drawing operation as it is directly related to thickness reduction of sheet metal. LDR depends upon properties of the friction condition between tools and blanks, lubricant

applied to diminish friction coefficient as well as punch diameter and filter radius (GmbH, 1998). This condition shows that friction plays an important role in influencing the thickness of blank sheet metal.

Friction can be helpful to control the material flow and form more uniform components without defects (Ramezani & Ripin, 2012). A study reported that the increase of friction coefficient would be beneficial as it reduces blank thickness at cup wall area considerably. Wall thickness of 1 mm is reduced to 0.871 mm for a theoretical condition without friction. However, the thickness declined when the friction increased 0.815 for µ=0.05, 0.796 for µ=0.1, and 0.748 for µ=0.15. Therefore, the friction force induced when applying 29 to 31 kN was sufficient to control the flow of the blank material without causing any fractures. However, too high friction can cause damage as necking and tearing are observed when further increase of friction is applied due to an excessive reduction of material thickness (Olguner & Bozdana, 2016).

High friction induction may also cause other unfavourable effects as in this case high friction may oppose the flow of the blank material specifically in the flange region during forming, eventually, increasing the thickness and causing defect in the formed parts like delayed cracking (Ramezani & Ripin, 2012) which occurred when the maximum BHF of 32 kN is applied. High load leads to an increase of the friction force (Lazarescu, Nicodim, & Banabic, 2015) in the intimate contact between the sliding surfaces (Sondur, Kabadi, & Mallapur, 2014). When high volume of friction is presented, the outward movement of the blank material specifically in the flange region in contact with the blank holder is restricted, hence, bulging the cup. Excessive bulging at the flange region will result in high thickness and cause delayed cracking. The friction force opposes the material outward flow, hence, a higher stress must be induced near the centre of the contact zone

of region 5 as illustrated in Figure 4.7. Therefore, drawing force needed must be larger to move the clamped blank material outwards (Schey, 1987).

An experiment was conducted to observe the cup condition when a higher BHF of 33 kN was implemented. The result is in agreement with the conclusion made by (Olguner & Bozdana, 2016) as necking and tearing were observed in the corner region of the cup as shown in Figure 4.8 due to excessive friction induced in the clamped flange region opposing the material flow, hence, higher drawing force was needed to push the material throughout the die, eventually cause excessive thinning in region 5.

The claim of reappearance of fracture when the maximum BHF of 32 kN was exerted due to high induction of friction is compatible with the results obtained in section 4.1 as the Nano lubricant tribological performance was considered to be totally deteriorated when subjected to the maximum BHF of 32 kN due to the occurrence of fractures after exiting non-crack ranges. Under the maximum BHF of 32 kN, the nanoparticles worsened and its capability in reducing friction prone to lessen, eventually, restricting the flange deformation and causing the thick thickness at this region and, eventually, causing delayed cracking.

Only thickness of 2wt% cups are analysed. The tribological performance of the nanolubricant plays a significant role in eliminating the fractures. Previous study (Tan, Aslian, Abe & Mori, 2016) shown that the optimum concentration of the same SiO_2 nanolubricant for the best tribological performance using the same uncoated tools in the deep drawing test was determined for 2 wt%. This also being the reason of why the cup's forming load for 1 and 3 wt% are not studied through this study.

4.3 Heights of peak and valley points along cup edge

Figure 4.9 illustrates the average peak and valley point heights along the cup edge measured from the bottom for different BHFs.
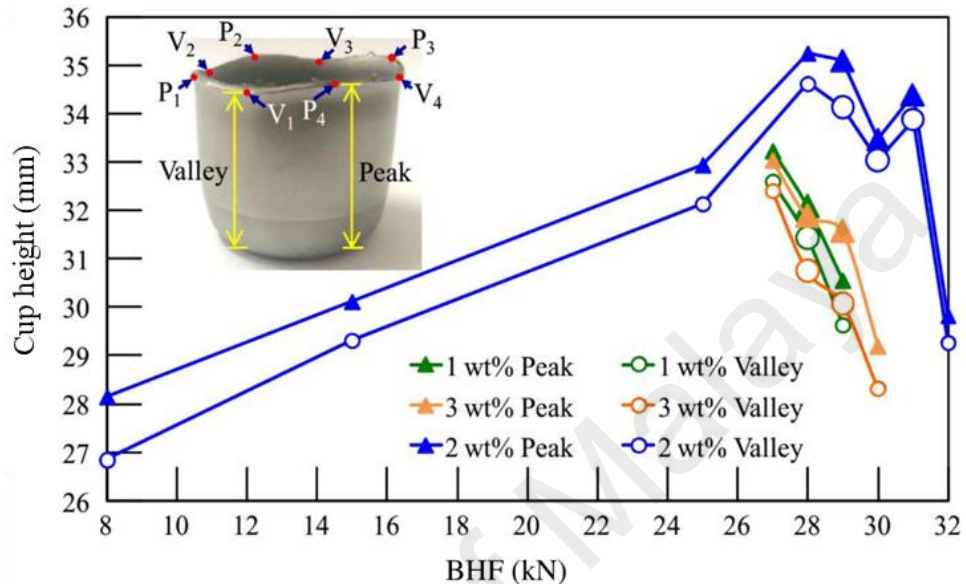
Figure 4.9: Average height of peak and valley points along cup edge for different BHFs

During deep drawing operation, a phenomenon called earing tends to occur where the edges of cups become wavy due to uneven metal flow in different directions and this phenomenon is directly related to planar anisotropy. Generally, earing which is one of the failures in deep drawing is caused by an inhomogeneity of radial strain along the circumferential direction in a blank sheet flange area (Patel, Dave, & Raval, 2015). Much work has been done in preventing earing due to its significant impact on production cost and efficiency. In deep drawing hollowware production, wasteful of material often occurs when larger blank than necessary must be used. Additionally, it may cause difficulties in ejecting products after a pressing operation.

From the experiment, it is obvious that 2 wt% concentration resulted in the largest elongated height compared to other concentrations (1 and 3 wt%). Overall, the trend

showed an increment in both points (peak and valley) of 2 wt% SiO_2 when the BHF increased from the minimum of 8 kN to the maximum of 28 kN, giving the highest peak of 35 mm before slightly decreasing within the crack free range from 29 to 31 kN. The pattern was then continued to decline sharply for BHF of 32 kN, causing reappearance of fracture. Logically, the longer is the waviness the thinner is the cup walls' thickness. Hence, this result is consistent with the cups' wall thickness distribution presented in Figure 4.5. The wall thickness around the cups' inner corner and side wall for BHF of 28kN with 2 wt% SiO_2 was the thinnest, leading to the largest, elongated height. The same trends were obtained for 1 and 3 wt% under elevated BHF, i.e. cracking at the maximum, elongated cup height, then no cracking with a slight rebound in height. Eventually, the cracks reappeared with a sharp decline in elongated height.

The decrement in cup elongation once entering higher BHF of non-crack range was due to the restricted deformation in the flange portion, resulting in the slightly increase in frictional force. In metal forming operation, friction between workpiece and tool is an imperative parameter influencing the material flow where in deep drawing the main source of friction is in the blank holder when the flange region of the blank being clamped between blank holder and circular die (Başpınar & Akkök, 2016).

As discussed in section 4.2, although the increase of friction coefficient has been proven to be effective in influencing the metal flow like reducing the blank thickness considerably (Olguner & Bozdana, 2016), too high friction may cause component defects like necking and tearing. Besides, too much friction may oppose the flow of blank material specifically in the flange region. High volume friction will oppose the outward movement of the blank material in the flange as this area is in contact between the die and blank holder, hence, bulging the region which prone to delayed cracking (Schey, 1987).

The bulged region showed that the material flow was restricted and this affected the component elongation and wall thickness.

The notion that high friction results in low material elongation is supported by the forming force results obtained in the section 4.4. The peak forming load was the smallest when exerted to 28 kN, hence, minimum friction was induced, leading to the largest elongated cup height and minimum side wall thickness respectively, featuring well improvement of formability. However, when the load was increased from 29~ 32 kN, the peaks forming load were rebounded, showing larger induction of friction resulting in the smallest elongated cup height and higher side wall thickness as shown in Figure 4.9 and Figure 4.5 respectively. High forming load leads to an increase of the friction force (Lazarescu et al., 2015). This trend show that large volume of friction restricts the material flow specifically in material height elongation and wall thickness.

From the figure 4.9, the cup heights for 1, 2 and 3 wt% continued to decrease sharply when subjected to 29, 32 and 30 kN respectively resulting in crack reformation due to Nanolubricant deterioration. Hence, the tribological properties of 1,2 and 3 wt% Nano lubricant totally deteriorated as the limit to encounter the effect of friction and maximum load-carrying capacity was achieved. The maximum amount of BHF needed to mitigate fracture was hardly influenced by the increase in SiO_2 concentration.

A study reported that the friction between the workpiece and the tools has both negative and positive effects. In some cases, friction can be convenient to control the material flow and form more uniform parts without defects. However, too high friction may oppose the material flow during forming that may cause defects in the formed components (Ramezani & Ripin, 2012) as occured when 29 , 32 and 30 kN were applied using 1,2 and 3 wt % respectively.

In this case, high load deteriorated the Nano lubricant performance, causing high induction of friction force in the flange region which eventually, influencing the material elongation. A study reported that the tribological properties of nanoparticles tend to diminish under heavy load (Thirumalaikumaran, 2017). As explained in the section 4.1, under high pressure, the special effects of nanoparticles like the lubricant film is to separate the contacting surfaces become thinner (Battez et al., 2007), hence the blank holder and die surfaces will have direct contact with the circular blank, leading to high induction of friction force.The nanoparticles also tend to crush during the sliding, eventually agglomerating and causing plough marks on the material resulting in friction induction and consequently component failure.

4.4 Forming force

Figure 4.10 presents the experimental punch force – displacement curves for different BHFs using 2 wt% SiO_2.
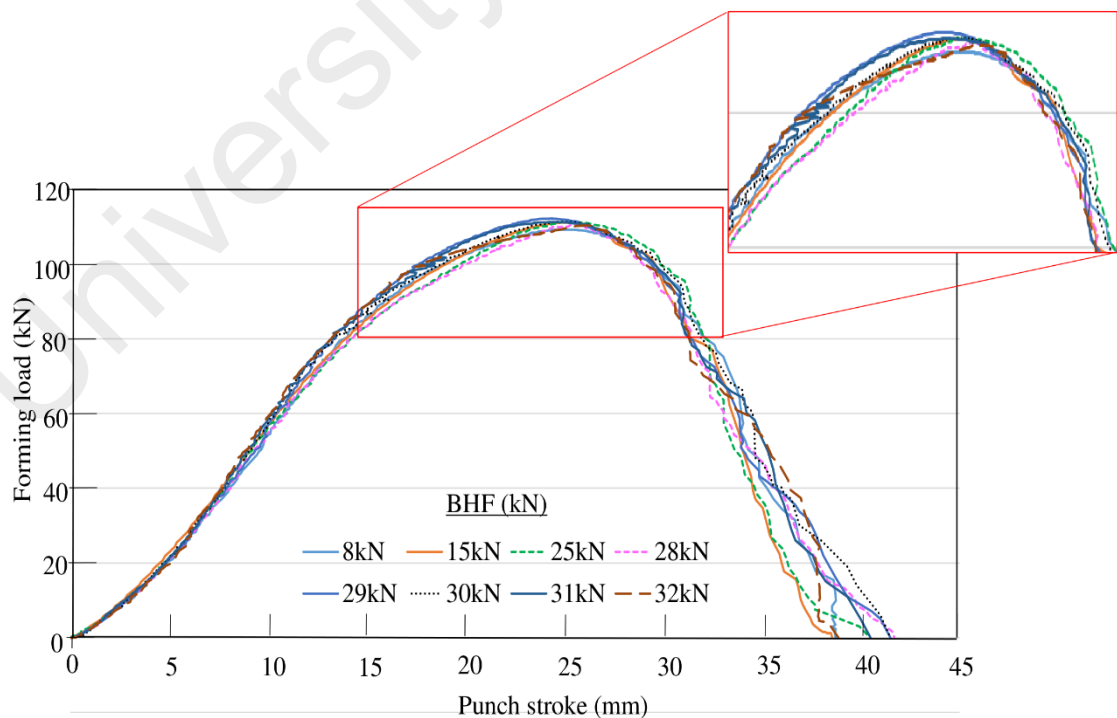

Figure 4.10: Forming loads for different BHFs using 2 wt% of SiO_2

It is clear that the punch load, in which the punch acted on the blank moderately increased at the early stage of process as the blank deformed by bending and decreasing until the die aperture was reached as a result of flange reduction. In fact, the load increased when the punch moved downwards due to the increase in strain on the metal and also because the material gets strain hardened, ramming the die and reaching the maximum value as friction due to hold down plate pressure as well as sliding prone to increase and decrease during the drawing before the load gradually decreased. This is due to the fact that after certain amount of drawing the amount of blank material beneath the hold down plate lessened.

In general, it could be concluded that the forming loads barely changed with the increasing BHF from 8 to 32 kN with the aid of Nano lubricant. A study reported similar results for deep drawing of ultra-high strength steel sheets using a similar Nano lubricant with an uncoated drawing die i.e. with 2 wt% SiO_2 (Tan, Aslian, Abe, & Mori, 2016). Under high contact pressure with the aid of excellent performance of the Nano lubricant, the ironing limit of cups made from aluminum alloy was successfully increased from 24.8% to 35.2% by suspending a mere 1.0 wt% of SiO_2 in oil with a kinematic viscosity of 170 mm2/s.

Figure 4.10 depicts that the forming load had not much influence at the early stage of the drawing process. However, at larger punch travels, the friction affected the required drawing force considerably. This is clearly seen as the peak load rebounded after 28 kN due to the slightly increase in frictional force. Friction is one of the most vital parameters, which influences the material flow and required load in bulk forming (Fereshteh-Saniee & Bayateefar, 2002; Saniee, Pillinger, & Hartley, 2004) and sheet forming processes (Robert & Wagoner, 1997).

Basically, larger punch load values are linked with larger global friction coefficient amount (Simões, 2012). This claim is supported by (Olguner & Bozdana, 2016) as they reported that the increase of friction coefficient significantly increased the needed forming load. Needed punch load was 27.48 kN for the theoretical condition without friction (μ=0). However, the value increased to 27.84 kN for μ=0.05, 31.2 kN for μ=0.1 and 34.92 kN for μ=0.25. From the test, it was observed that the rise of coefficient of friction from 0 to 0.25, attributed to the increment of forming load more than 30%. Therefore, this study outcome supported the claim that friction was a factor influencing the forming load.

The minimum friction was induced when 28 kN was applied as the graph illustrates minimum peak load compared to other BHFs, resulting in the largest, elongated cup height (Figure 4.9) and minimum side wall thickness (Figure 4.5) respectively, featuring well improvement of formability for this material. The addition of BHF from 29 ~32 kN increased the friction resulting in significant rebounding in forming load.

4.5 Austenite and α′-martensite stability

The X-ray diffraction pattern under elevated BHF from the minimum of 8 to 32kN with 2 wt% SiO_2 is shown in Figure 4.11. The measurement was taken at a point located approximately 1 mm below the cup edge at the outer surface. In as-received condition, the microstructure of the blank was completely unstable austenite (FCC) before transforming to metastable ε-martensite (HCP) and eventually to α′-martensite (BCC) after undergoing deep drawing operation. In Figure 4.11, there are variations in the peak intensities and their positions due to the phase transformations and the sizes of crystal structures (Hossain, Pahlevani, Quadir, & Sahajwalla, 2016) after subjected to an elevated BHF.

Before compression testing, the blank specimen showed austenitic peaks at (111), (200) and (220) diffraction positions. As the compressive load was increasing from 8 to 28 kN, the austenite peak started decreasing and the ε- and α′- martensite peak at (110) and (211) started increasing. A similar trend was reported by (Hossain et al., 2016) as the peak during austenite phase decreased while martensite phase increased when exerted from 0 MPa to 2500 MPa. However, the trend changed significantly when entering crack-free BHF range as the austenite peak started to increase and ε- and α′- martensite started to decrease.
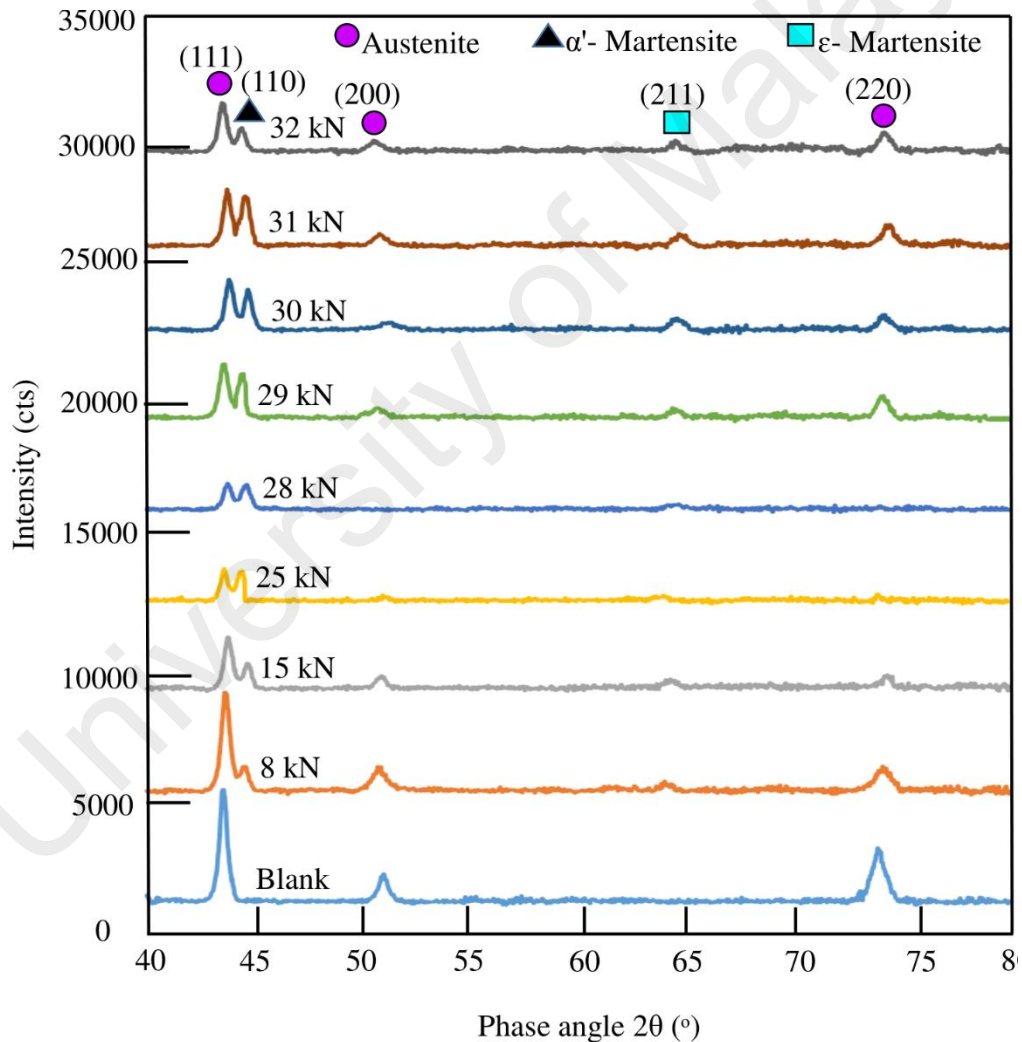
Figure 4.11: X-ray diffraction pattern under elevated BHF for 2 wt% of SiO$_2$

According to the XRD analysis, the sum of photons collected by the detector at a phase angle within the pre-set time interval was counted as intensity (cts). There are few factors influencing the peak intensity like sample's surface texture, etc., and these factors are not constant under elevated BHFs. Under the influence of the factors, the peak intensity for all phases of austenite (FCC), ε-martensite (HCP) and α′-martensite (BCC) was reduced and the minimum value at BHF of 28 kN was reached as shown in Figure 4.12.

The intensity rebounded at BHF of 29 kN and maintained at the same level after that. To exclude the influence of these factors, it is more accurate to obtain the distribution of relative intensity (%) to the largest peak, i.e. the peak intensity for α′-martensite 44° at each BHF as shown in Figure 4.13.

Figure 4.12: Peak intensity distribution

Figures 4.12 and 4.13 show the peak intensity (cts) distribution and the relative intensity (%) distribution respectively of all three phases transformation at different phase angles (2θ) under elevated BHF for 2 wt% SiO_2. The value of peak (cts) and relative (%) are automatically measured by XRD machine.

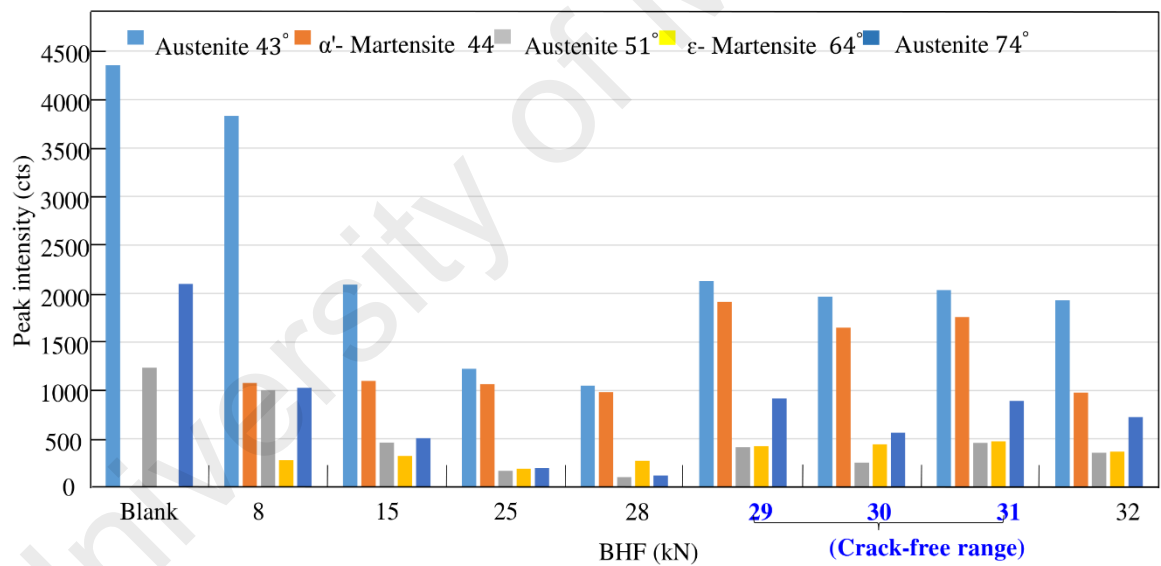As shown in Figure 4.13, at the minimum BHF of 8 kN, the relative intensity of α′-martensite rose markedly from 28.1% to a peak of 93.7% at BHF of 28 kN leading to the crack appearance. The pattern changed as the intensity of α′-martensite reduced slightly to 89.9% at BHF of 29 kN and remained at the same level within the crack-free range before declining significantly to 50.7% at BHF of 32 kN, resulting in the reformation of cracks. The rebound in the relative intensity of α′-martensite beyond 28 kN was due to the restricted deformation in the flange portion resulting in the slight increase in frictional force.

The BHF enhancement influenced the relative intensity of austenite at phase angles of 51° and 74° as the value decreased when subjected to 8 kN to 28 kN resulting in crack formation. The smallest relative intensity was acquired at BHF of 28 kN. The relative intensity strongly rebounded at BHF of 29 kN and remained at the same level within the crack-free range before declining after exiting the crack-free range at 32 kN. The decrease in austenite relative intensity at both phase angles was mainly due to the transformation of the metastable austenite microstructure into more stable ε- and α′-martensite induced by deformation at elevated BHF. Under extreme operating conditions, when the pressures on the substrate are high enough, the austenite can subsequently be transformed to the more stable martensite phase (De Knijf, Nguyen-Minh, Petrov, Kestens, & Jonas, 2014; Hossain et al., 2016; Litovchenko et al., 2016).

A study reported that the amount of austenite contained in a high carbon steel specimen prior compression was about 59-60%. However, the amount of austenite reduced significantly after subjected to 2000 MPa to 2500 MPa at room temperature. At 2000 MPa, the amount of austenite decreased to approximately 18% and at 2500 MPa to below 10% (Hossain et al., 2016). As a result of the martensitic transformation phenomenon, the amount of austenite decreased gradually as the stress increased.
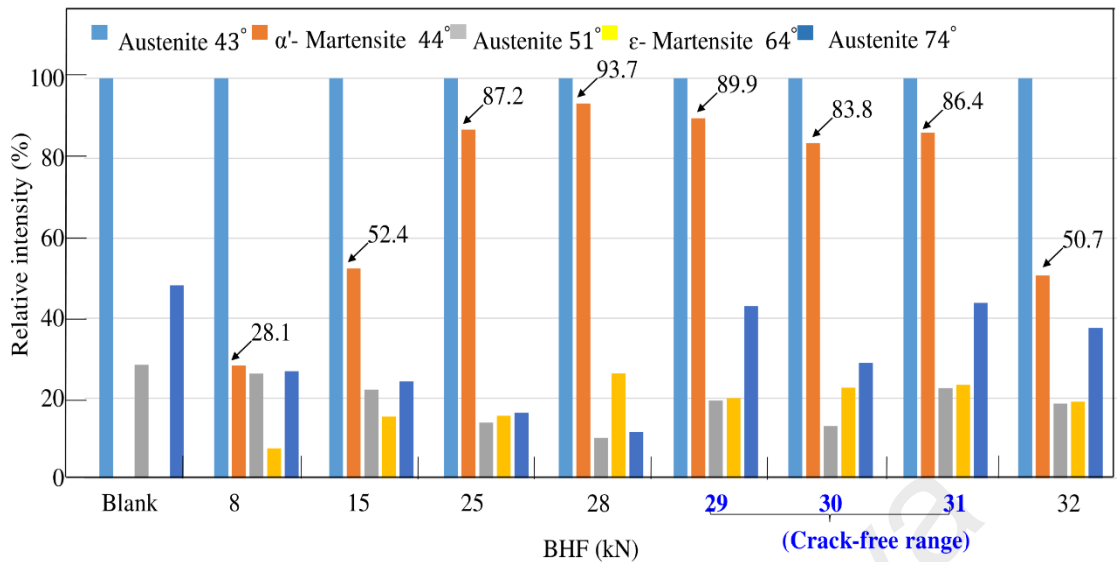
Figure 4.13: Relative intensity (%) of austenite andε – and α′-martensite under elevated BHF for 2 wt% SiO₂

Figure 4.14 presents the volume fraction distributions of austenite and ε and α′-martensite under the elevated BHF for 2 wt% SiO_2. The ratio of integrated intensities was used to estimate the volume faction (Chang & Gan, 1987). Below is the example of volume fraction for α′-martensite:

$$\frac{I_{\alpha'}}{I_{\gamma} + I_{\alpha'} + I_{\varepsilon}} \times 100 \qquad Eq.\,4.1$$

Where I_{γ} is total integrated intensities for austenite at all phase angles, $I_{\alpha'}$ is integrated intensity for α′–martensite and I_{ε} is integrated intensity for ε−martensite. From the volume fraction distributions graph, the maximum of 100% austenite was measured due to no compressive force exerted on the blank. At low compressive stress of 8 kN, the austenite fraction did not vary significantly because the compressive stresses were lower than the corresponding activation energy needed for phase transformation. The content of austenite decreased remarkably to below 40% when subjected to 28 kN, leading to crack formation.

Studies show that when the austenite reach sufficient energy from the induced stress, randomly spaced overlapping stacking faults create ε- martensite (Angel, 1954; Brooks, Loretto, & Smallman, 1979a). The α′- martensite phase nucleates at the intersections of shear bands , i.e. dislocation pile – ups on closely spaced slip planes (Brooks et al., 1979a; Brooks, Loretto, & Smallman, 1979b; Suzuki, Kojima, Suzuki, Hashimoto, & Ichihara, 1977). As a result of the transformation phenomenon, the amount of austenite drops moderately as the stress applied is increased.

As mentioned in the sub section 2.3.4, low nickel content in stainless steel contributes to fracture. Insufficient nickel content reduces austenite stability, hence decrease stacking fault energy (SFE) which result to fracture. However, nickel content is not a concern in this study as the nickel amount in the blank sheet is similar. The blanks used are made from the same batch of production (same lot number). Therefore, the nickel content in these blanks are the same and were treated as constant across the study.

Studies (Hansen & Pradhan, 1981; Jin Huang, 2004; Koo, 1977) observed that the martensite volume fraction (MVF) is a dominant factor in controlling strength and ductility. Under elevated BHF, the volume fractions of ε- and α′-martensite moderately rose and reached the maximum values at BHF of 28 kN due to the stress induced martensitic transformation. The trend changed once entering the crack-free BHF range as the volume fraction of α′-martensite was significantly reduced by half. The fraction slightly increased within the range before decreasing sharply when exiting the range. The pattern is similar to the one depicted in Figure 4.12.

The content of α′- martensite increased gradually to the maximum of 48% as the stress applied was increased when subjected to 28 kN. This may have occurred as the structures gained sufficient energy for phase transformation from austenite to α′- martensite when subjected to 28 kN load (Hossain et al., 2016). The change in ε- martensite content was

not significant but the α′- martensite content increased remarkably. This shows that the transformation process involves both austenite to ε- martensite and austenite to α′- martensite transformations and enables strain hardening.
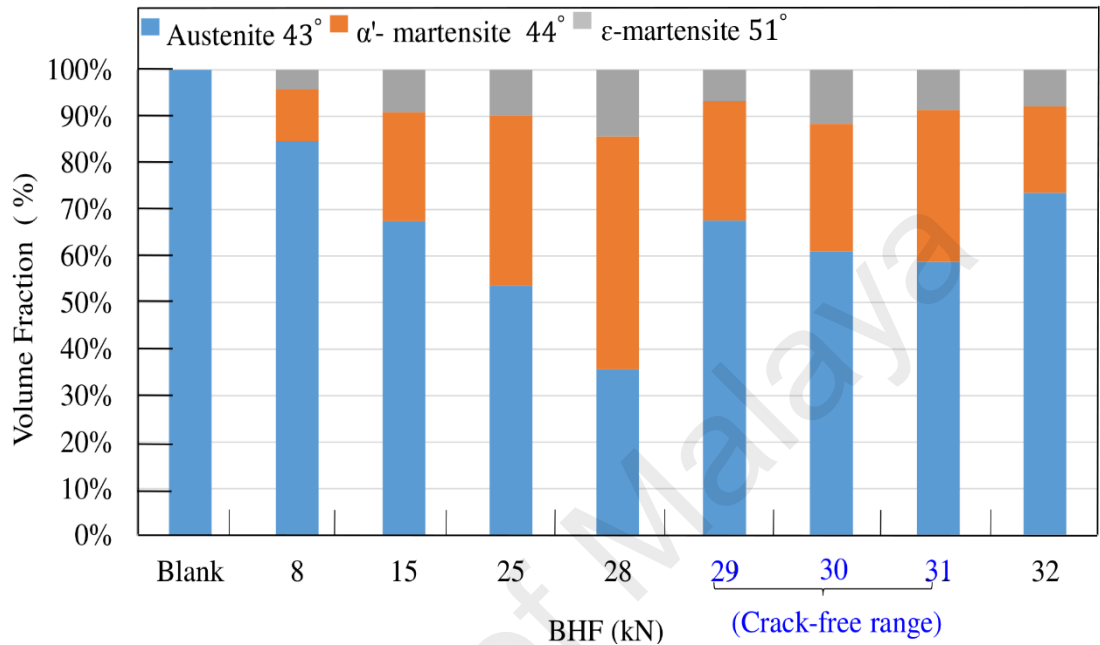
Figure 4.14: Volume fraction distributions of austenite and ε – and α′- martensite under elevated BHF for 2 wt% SiO₂

Figure 4.15 presents the relative intensity (%) distribution of austenite and ε and α′- martensite at different phase angles (2θ) and elevated BHF for 1 wt% SiO_2. The highest relative intensities for ε- and α′-martensite were acquired at BHF of 27 kN, i.e., immediately before fracture disappearance. The intensity declined moderately when entering crack-free BHF and decreased sharply after that, resulting in crack reformation. In comparison, the trend obtained for 1 wt% was similar with 2 wt%. However, the relative intensities for strain induced ε- and α′-martensite with 1 wt% SiO_2 were lower than the ones obtained with 2 wt% within the same BHF rangedue to the lower amount of deformation as a result of the difference in lubrication performance.
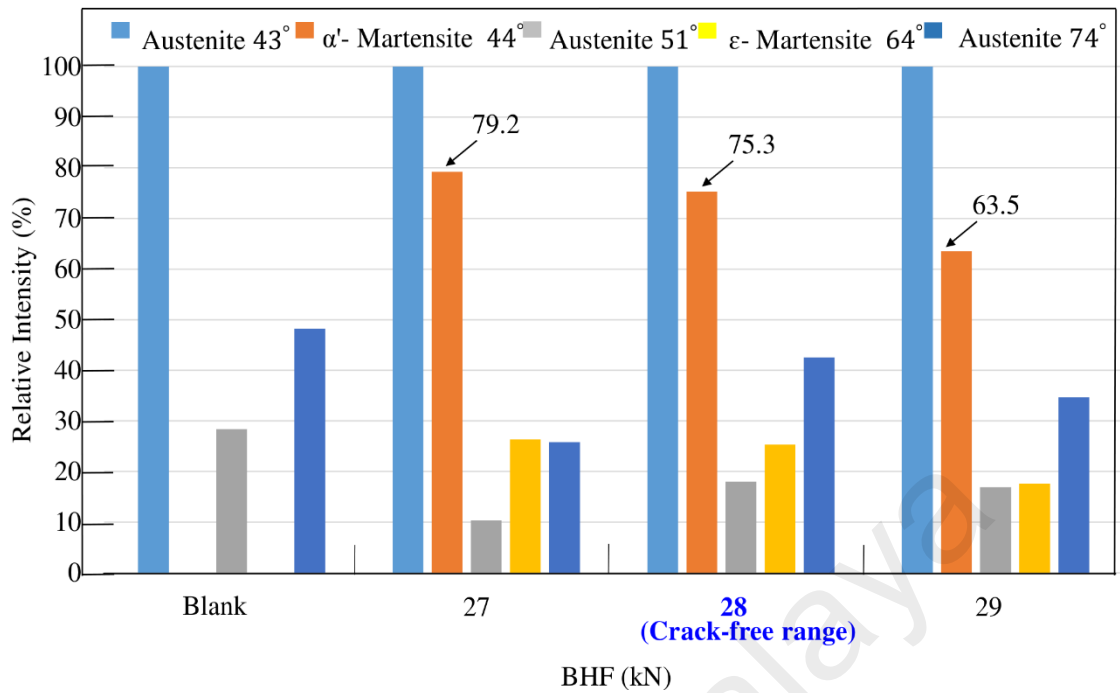
Figure 4.15: Relative intensity (%) of austenite and ε – and α′-martensite under elevated BHF for 1 wt% SiO₂

Figure 4.16 illustrates the relative intensity (%) distribution of austenite and ε and α′-martensite at different phase angles (2θ) under elevated BHF for 3 wt% SiO₂. From the graph, it is clear that the highest relative intensity for α′-martensite was obtained at BHF of 27 kN, i.e., the BHF right before the cracks disappeared.

The intensity declined moderately when entering the crack-free range at 28 and 29 kN prior decreased sharply, resulting in the reformation of cracks at BHF of 30 kN. Overall, this trend is similar to the results in Figure 4.13 and 4.15 for 2 wt% and 1 wt% SiO₂, respectively. However, the relative intensity of the strain induced α′-martensite for 3 wt% SiO₂ was lower than for 2 wt% but higher than for 1 wt% within the same BHF range due to the different amounts of deformation as a result of the change in lubrication performance.
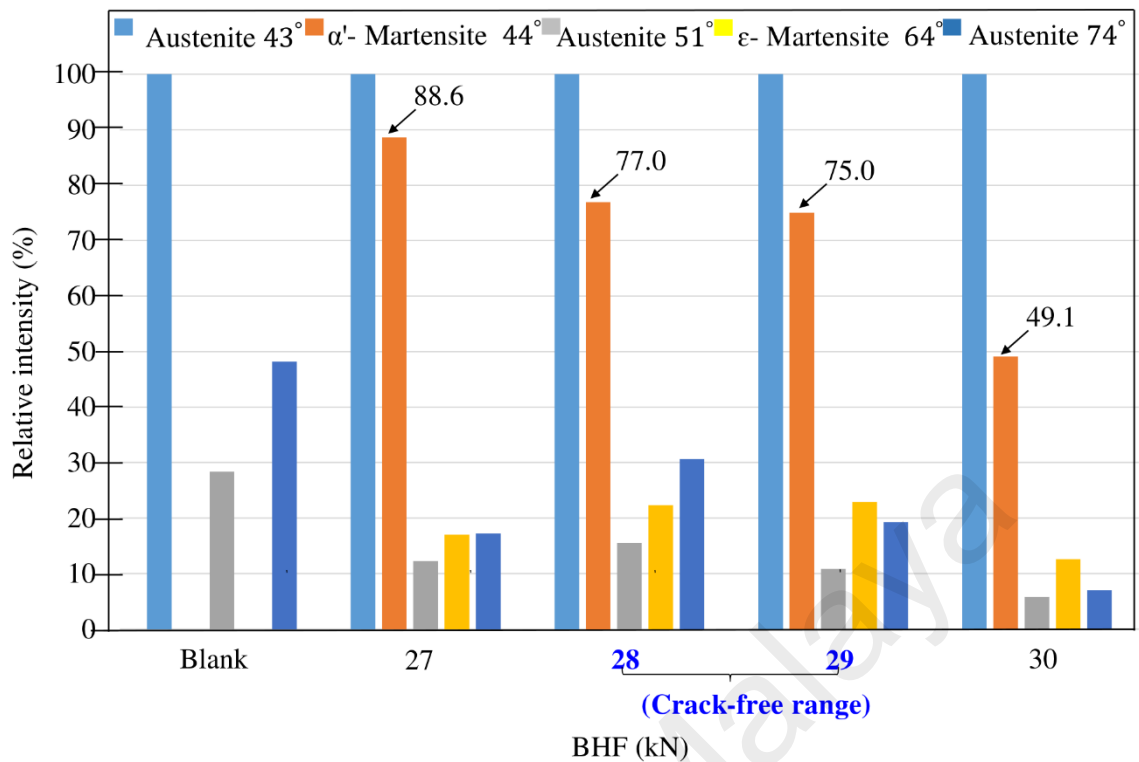
Figure 4.16: Relative intensity (%) of austenite and ε – and α′-martensite under elevated BHF for 3 wt% SiO₂

4.6 Residual stress measurement with X-ray diffraction

The residual stresses in the cup wall were mainly caused by the material unbending as the material left the draw die profile (Saito & Shimahashi, 1979). In general, the residual stresses are caused by mechanical working processes that determine the material deformation and modify the shape of part or the properties of its material (Brabie, 2005; Hauk, 1997). In the case of metal sheets deep drawing, residual stresses are developed through the incompatibility between the permanent material deformations and occur in conditions in which some dissimilarities exist between the deformation states of different materials (El Sherbiny et al., 2014).

Figure 4.17 shows the tangential residual stresses for all crack-free drawn cups formed with 1, 2, and 3 wt% SiO₂. All stresses were measured with X-ray diffraction below a valley point along the outer surface of cup edge. Tangential residual stresses were

considered the most significant ones because fractures propagate vertically down the cylindrical drawn cup walls (Simões, 2012). Inhomogeneous deformation and stress distribution caused during the drawing process can develop strong tangential residual stress in the wall of the drawn cup (Jung et al., 2017).

From the test, it was observed that, despite the high tensile residual stresses along the outer surfaces, no fracture was observed in these crack-free cups. The result is compatible with the outcomes obtained by other studies, stating that the tangential residual stress contained in the drawn cups are compressive at the cup's inner surface and tensile at the outer surface (Danckert, 1995; Papula, Saukkonen, Talonen, & Hänninen, 2015). The bending and re-stretching at the die shoulder primarily determine the tensile residual stress at the outer surface and the compressive stresses at the inner surface. The formation of the tangential or also known as circumferential tensile stress is due to the compression deformation in the tangential direction in the flange region while being pulled in the radial direction. The tangential compressive stress results from the fact that the blank has to lessen its radius in order to fit inside the die's cavity (Simões, 2012). After undergoing deep drawing operation, the punch load is unloaded, but complete elastic recovery is not possible due to restraining as a container (Sudo, Iwase, Hattori, & Nakajima, 2005).
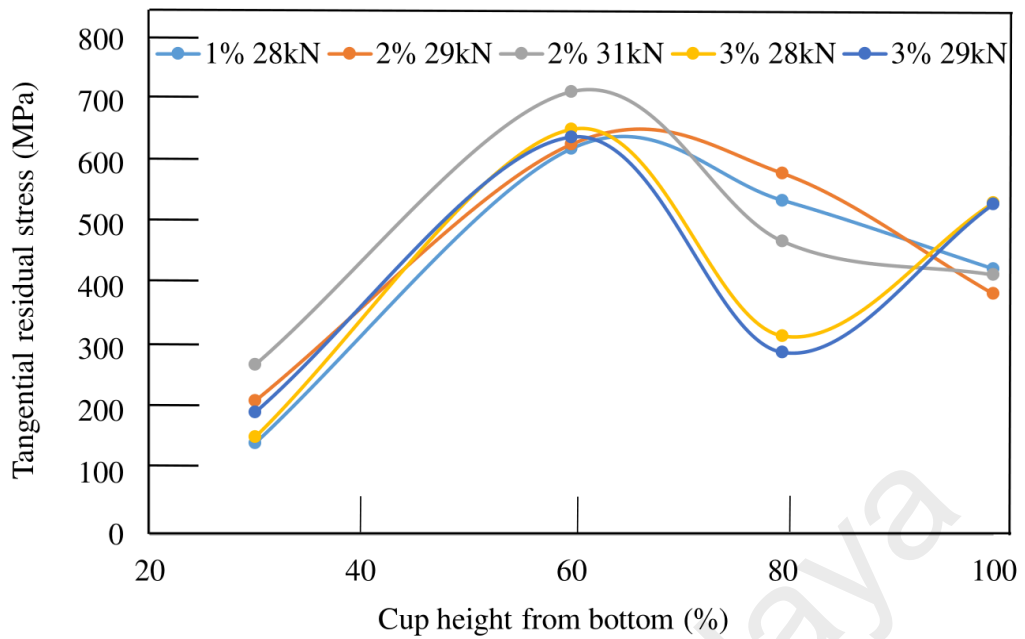
Figure 4.17: Tangential residual stresses measured with X-ray diffraction for all crack-free drawn cups formed with 1, 2, and 3 wt% SiO

From Figure 4.17, residual stresses distribution for all crack-free cups were similar as the tensile residual stress increased along with the height and reached a peak at around 50-60% height. This pattern is in agreement with previous studies (Papula, 2015; Papula, Talonen & Hänninen, 2014) as the maximum value of the residual stress is within this range.

After that point, the tensile residual stress values reduced with further increase in cup height up to 100%. For 2 wt%, the increase in BHF significantly reduced the residual stress at 80% height, leading in a lower stress gradient in the upper portion of the cup, which was favorable for eliminating delayed cracks.

A similar trend was observed for 3 wt% when the BHF increased from 28 to 29 kN as the stress value was significantly reduced at 80% height, resulting in the reverse stress gradient. This result showed that the optimum BHF to minimize the tangential residual stress for 2 wt% and 3 wt% were 31 kN and 29 kN respectively. However, the degree of

increase in residual stress at 100% height for 3 wt% was too high and resulted in the reappearance of cracks when the BHF increased out of the crack-free range. This outcomes is acceptable as a couple of study concluded that delayed cracking occurrs at an excessive tensile residual stress level (Berrahmoune, Sophie Berveiller, Karim Inal, Etienne Patoor, et al., 2006; Chen, Leng, & Shao, 1988). (Jung et al., 2017) and (Guo, Post, Groen, & Bleck, 2011) claimed that the crack incubation time representing the resistance to delayed cracking as the higher is the residual stress, the shorter time is required for the fracture to occur. Hence, this statement is consistent with the results obtained in Table 4.2 as the duration for first crack to form for 3 wt% is four times quicker than 2 wt%.

Obviously, the residual stress changed beyond 80% cup height. The compression in this portion rose with elevated BHFs, leading to greater deformation because the flange region equivalent to 80~100% cup height was initially in contact with the blank holder and die before being pulled into the die cavity. Additionally, the pressure enhanced further because of the decreasing area of contact between the tool surface and the blank during flange pulling. Hence, the effective holding force acting on the flange increased during the metal forming process, resulting in residual stress changes beyond 80% cup height.

4.7 Residual stress measurement by ring slitting method

The tangential residual stresses in cylindrical drawn cups were also measured using a ring slitting method based on residual stress relaxation (Prime, 2018).The slitting method, also known as crack compliance, is a powerful and widely used method for measuring residual stress (Cheng & Finnie, 2007; Prime, 2015). One of the ultimate benefits of this method in comparison to X-ray diffraction is that residual stresses that contained in the cups prior to cracking can also be measured from the cracked areas of the cups (Papula, 2015).

The crack-free cups were sectioned into 4 rings in different heights of 30,60, 80 and 100% from cup bottom in a water bath to prevent frictional heat before slitting in the longitudinal direction to obtain an opening gap. The difference between the ring diameters , before and after slitting, provides a direct measure of the delayed crack phenomenon, and indirectly, of the residual stress in the tangential direction induced in the formed cup (Demeri et al., 2000).

The rings open gap distance, increased with height and was the largest at 60% height as shown in Figure 4.18. The largest tensile residual stress was induced at 60% cup height. However, the gap distance declined with further increase in height. This result is consistent with the results obtained using X-ray diffraction as the maximum residual stress was observed at 60% cup height as shown in Figure 4.17.
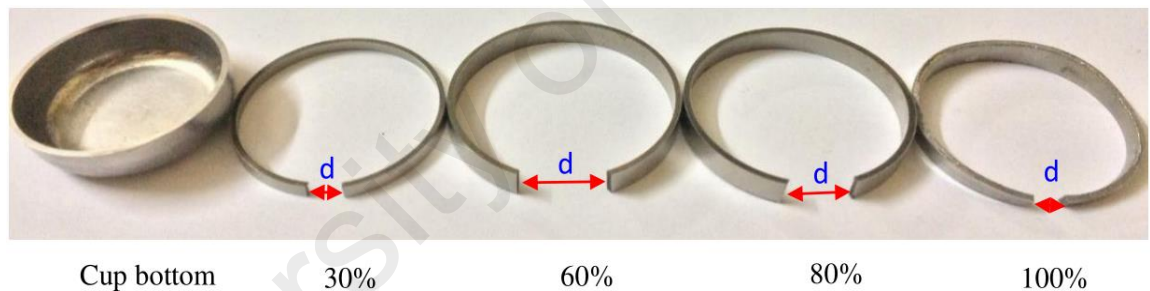
Figure 4.18: After: Slit cylindrical drawn cup into 5 different heights

Figure 4.19 presents a comparison of the tangential residual stress results between the X-ray diffraction analysis and ring slitting method for BHF of 29 kN and 31 kN with 2 wt% SiO$_2$. Overall, the residual stresses obtained with these methods are in fairly agreement for the specified conditions. Approximately 13% difference of residual stress measured between these 2 methods as the XRD analysis measured the residual stress on a single point along the outer cup surface while the ring slitting method considered the open gap of a slit ring at a similar height. Regardless of this difference, both results were

acceptable as the tangential residual stress results were closed, leading to similar trend for both methods.
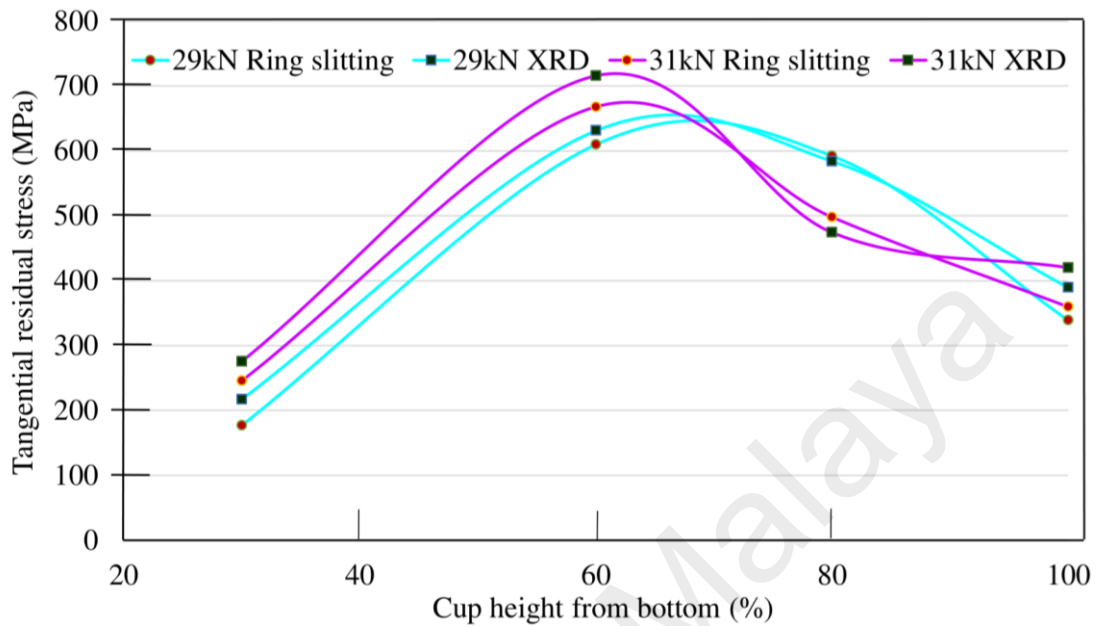
Figure 4.19: Comparison of tangential residual stress results between XRD analysis and ring slitting method for BHF of 29 kN and 31 kN with 2 wt% SiO₂

Figure 4.20 shows a comparison of the longitudinal stresses at 100% of the crack-free drawn cups measured with X-ray diffraction analysis. Cylindrical cup wall is primarily experiencing a longitudinal tensile stress as the punch transfers the drawing force through the cup walls and through the flange as it is drawn into the die cavity (Hussaini, Singh, & Gupta, 2014). In this study the longitudinal stresses induced in the wall of the crack-free cups were all compressive.

Overall, the increment in BHF influenced the compressive residual stress as its magnitude increased. The compressive residual stress increased 3 times for 2 wt% when the BHF increased from 29 to 31 kN. At BHF of 29 kN, the residual stress magnitude escalated greatly with increasing concentration from 2 to 3 wt%. The increment in compressive residual stress as the concentration increased tallied with the results obtained in Figure 4.9 as the elongated cup heights for 2% was much longer that 3 wt% under the

same BHF of 29 kN i.e., greater height for higher stress. However, the stress magnitude at BHF of 28 kN was hardly influenced by increasing the concentration from 1 to 3 wt%, as the cup heights in both cases were almost the same.

The longitudinal or delayed cracks were influenced by tangential residual stresses due to the effect of high tensile stress in cup's outer surface but not the high compressive longitudinal residual stress. (Simões, 2012) claimed that residual stresses in tangential direction are considered the most important one because delayed cracks propagated vertically down the cylindrical cup walls. He added that the shear on material mainly caused by the tangential force. A study concluded that tensile residual stress in tangential direction is a fundamental factor of the delayed cracking of twinning – induced plasticity steel , using the neutron diffraction method (Hong et al., 2014).

Residual tensile stress always occurs with residual compressive stress. However, tensile residual stress can have an adverse effect on material fatigue performance while compressive residual stress can significantly increase fatigue resistance. Number of studies concluded that tensile residual stress induces environmentally assisted cracking initiation, leading in greater risk of damage (Hashmi, 2014; Nedoseka, 2012; Todinov, 2006; Ye, 2015). However, compressive residual stresses are usually having a great influence since they reduce total stresses and minimizing fatigue crack initiation as well as increase wear resistance (Doremus et al., 2015; Todinov, 2006). However, the tangential tensile residual stress increases under rising compressive longitudinal residual stress due to stress equilibrium.
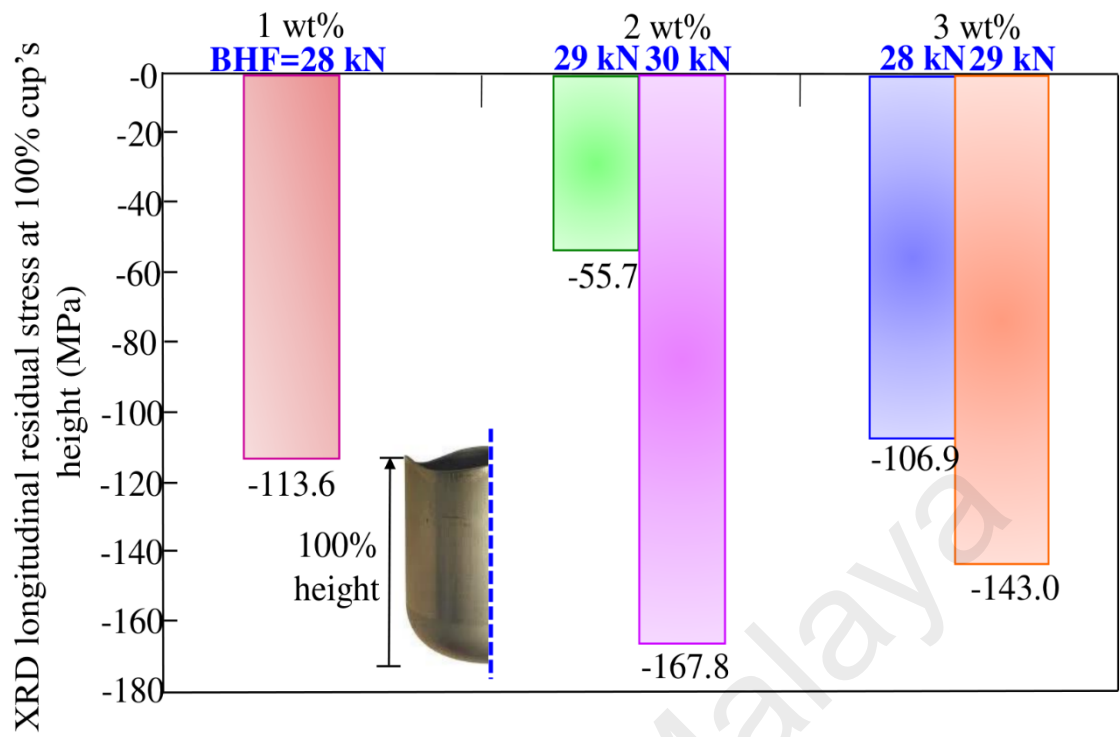
Figure 4.20: Comparison of longitudinal stress at 100% height of cylindrical crack-free cups measured with X-ray diffraction analysis

CHAPTER 5: CONCLUSION AND RECOMMENDATIONS

5.1 Conclusion

Several conclusions can be drawn through the effect of using extreme blank holding force (BHF) in the deep drawing of SUS304 cylindrical cups aided by 1, 2 and 3 wt% SiO_2 Nano lubrication at limiting draw ratio at room temperature.

First, delayed cracking of the deep drawn SUS304 cylindrical cups are successfully prevented by applying BHF approximately 3.6~3.9 times larger than the minimum force needed to avoid wrinkles with 2 wt% SiO_2 nanolubricant. Second, the largest crack-free BHF range is acquired using 2 wt% SiO_2 nanolubricant at BHF = 29–31 kN. The range becomes smaller when applying minimum concentration of 1 wt% SiO_2 Nano lubricants at BHF = 28 kN due to low tribological performance. However, the range is not successfully widening when the concentration increases to 3 wt% SiO_2 at only 28-29 kN due to the deteriorating nanolubricant functionality. Third, the elimination of delayed cracks is due to lower tensile residual stress gradient generated along the outer cup surfaces beyond 80% height, resulting in the slight increase in frictional force in the radial direction along the flange surface when entering the crack-free range. Next, the slight increase in adjusted coefficient of friction is proven by the rebound in sidewall thickness, elongated height, drawing force and relative intensity of α′-martensite when entering the crack-free BHF range. Fifth, the crack reformation after exceeding crack-free range is attributed to the excessive rise in tensile residual stress in the circumferential direction along the cup's outer surface at 100% height, resulting in the larger compressive longitudinal residual stress. Lastly, the time taken for the first crack to occur increases greatly when the BHF increases. The number of cracks for 2 wt% SiO_2 is smaller than for 1 wt% and 3 wt% when subjecting to the same BHF range.

5.2 Recommendation

In industrial applications, there are many ways to increase the BHF like increasing the spring constant and the number of coil springs for single action presses or by increasing the hydraulic pressure of the holding ring for double action presses. The crack – free holding pressure range for other blank sizes has a similar initial blank thickness which can be computed by dividing the BHF range with the top surface area of the die in contact with the blank acquired in the study. The crack – free BHF range for other drawn cup sizes can be calculated by multiplying the calculated holding pressure with the contact area obtained from the new tooling geometries.

For future research, different material such as copper alloy and other SUS grades can be used using same method in deep drawing of cylindrical cups.

REFERENCE

Afshin, E., Kadkhodayan, M. J. M., & Design. (2015). An experimental investigation into the warm deep-drawing process on laminated sheets under various grain sizes. *87*, 25-35.

Akbulut, M., 2012. Nanoparticle-based lubrication systems. *J. Powder Metall. Min*, *1*(1), pp.1-3.

Akiyama, E. (2012). Evaluation of delayed fracture property of high strength bolt steels. *ISIJ international, 52*(2), 307-315.

Angel, T. J. J. I. S. I. (1954). Formation of martensite in austenitic stainless steels. *177*, 165-174.

Bandyopadhyay, K., Panda, S., Saha, P., Baltazar-Hernandez, V., Zhou, Y. J. M. S., & A, E. (2016). Microstructures and failure analyses of DP980 laser welded blanks in formability context. *652*, 250-263.

Başpınar, M., & Akkök, M. (2016). Modeling and simulation of friction in deep drawing. *Journal of Tribology*, *138*(2).

Battez, A. H., González, R., Felgueroso, D., Fernández, J., del Rocío Fernández, M., García, M., & Penuelas, I. J. W. (2007). Wear prevention behaviour of nanoparticle suspension under extreme pressure conditions. *263*(7-12), 1568-1574.

Battez, A. H., González, R., Viesca, J., Fernández, J., Fernández, J. D., Machado, A., . . . Riba, J. J. W. (2008). CuO, ZrO2 and ZnO nanoparticles as antiwear additive in oil lubricants. *265*(3-4), 422-428.

Battez, A. H., Viesca, J., González, R., Blanco, D., Asedegbega, E., & Osorio, A. J. W. (2010). Friction reduction properties of a CuO nanolubricant used as lubricant for a NiCrBSi coating. *268*(1-2), 325-328.

Bending,Forming,Deep Drawing and Spinning. (2013). *Deepa drawing manufacturing*. Retrieved from http://www.roymech.co.uk/Useful_Tables/Manufacturing/Deep_Drawing.html

Berrahmoune, M., Berveiller, S., Inal, K., Moulin, A., Patoor, E. J. M. S., & A, E. (2004). Analysis of the martensitic transformation at various scales in TRIP steel. *378* (1-2), 304-307.

Berrahmoune, M., Berveiller, S., Inal, K., & Patoor, E. (2006). Delayed cracking in 301LN austenitic steel after deep drawing: Martensitic transformation and residual stress analysis. *Materials Science and Engineering: A, 438*, 262-266.

Berrahmoune, M., Berveiller, S., Inal, K., Patoor, E. J. M. S., & A, E. (2006). Delayed cracking in 301LN austenitic steel after deep drawing: Martensitic transformation and residual stress analysis. *438,* 262-266.

Berrahmoune, M. R., Berveiller, S., Inal, K., & Patoor, E. (2006). *Residual stress state at different scales in deep drawn cup of unstable austenitic steel.* Paper presented at the Materials science forum.

Bhaumik, S., Prabhu, S., & Singh, K. J. J. A. i. T. (2014). Analysis of tribological behavior of carbon nanotube based industrial mineral gear oil 250 cSt viscosity. *2014*.

Bill Lucas., G. M., and David Abson (Producer). (2000, January/February). DEFECTS - HYDROGEN CRACKS IN STEELS - IDENTIFICATION. Retrieved from https://www.twi-global.com/technical-knowledge/job-knowledge/defects-hydrogen-cracks-in-steels-identification-045

Birnbaum, H. K., Sofronis, P. J. M. S., & A, E. (1994). Hydrogen-enhanced localized plasticity—a mechanism for hydrogen-related fracture. *176*(1-2), 191-202.

Brabie, G. (2005). Residual stresses generated by materials transformation processes. *Iasi (Romanian): Junimea*.

Brooks, J., Loretto, M., & Smallman, R. J. A. M. (1979a). Direct observations of martensite nuclei in stainless steel. *27*(12), 1839-1847.

Brooks, J., Loretto, M., & Smallman, R. J. A. M. (1979b). In situ observations of the formation of martensite in stainless steel. *27*(12), 1829-1838.

Canter, N. J. T., & Technology, L. (2009). Challenges in formulating metal-forming fluids. *65*(3), 56-63.

Carcel, A., Palomares, D., Rodilla, E., Puig, M. P. J. M., & design. (2005). Evaluation of vegetable oils as pre-lube oils for stamping. *26*(7), 587-593.

Chang, L., Gan, D. J. M. S., & Engineering. (1987). The effects of grain boundary carbides on the low cycle fatigue properties of type 316 stainless steel. *95*, 125-136.

Chen, F.-K., Tseng, P.-C. J. J. o. m. s., & engineering. (2005). Deformation analysis of side-wall curl in the sheet-metal forming of flanged channels. *127*(2), 369-375.

Chen, Q., Leng, X., & Shao, E. J. W. (1988). Influence of microstructure and residual stress on the stages of case crushing. *122*(1), 45-55.

Cheng, W., & Finnie, I. (2007). *Residual stress measurement and the slitting method*: Springer Science & Business Media.

Chinas-Castillo, F., & Spikes, H. J. J. o. t. (2003). Mechanism of action of colloidal solid dispersions. *125*(3), 552-557.

Choi, Y., Hwang, Y., Park, M., Lee, J., Choi, C., Jung, M., . . . nanotechnology. (2011). Investigation of Anti-Wear and Extreme Pressure Properties of Nano-Lubricant Using Graphite and Ag Nanoparticles. *11*(1), 560-565.

Danckert, J. (1994). The residual stress distribution in the wall of a deep-drawn and ironed cup determined experimentally and by FEM. *CIRP Annals-Manufacturing Technology, 43*(1), 249-252.

Danckert, J. J. C. a. (1995). Reduction of the residual stresses in a deep-drawn cup by modifying the draw die profile. *44*(1), 259-262.

Davis, J. R. (1994). *Stainless steels*: ASM international.

Davis, J. R. (2000). *Alloy digest sourcebook: stainless steels*: ASM international.

De Knijf, D., Nguyen-Minh, T., Petrov, R., Kestens, L., & Jonas, J. J. J. J. o. A. C. (2014). Orientation dependence of the martensite transformation in a quenched and partitioned steel subjected to uniaxial tension. *47*(4), 1261-1266.

Demeri, M. Y., Lou, M., & Saran, M. J. (2000). *A benchmark test for springback simulation in sheet metal forming* (No. 2000-01-2657). SAE Technical Paper

Doremus, L., Cormier, J., Villechaise, P., Henaff, G., Nadot, Y., Pierret, S. J. M. S., & A, E. (2015). Influence of residual stresses on the fatigue crack growth from surface anomalies in a nickel-based superalloy. *644*, 234-246.

El Sherbiny, M., Zein, H., Abd-Rabou, M. J. M., & Design. (2014). Thinning and residual stresses of sheet metal in the deep drawing process. *55*, 869-879.

Fereshteh-Saniee, F., & Bayateefar, H. (2002). *Experimental comparison of different friction tests in bulk metal forming.* Paper presented at the Proceedings of the 7th International Conference "Technology of Plasticity", Yokohama.

Figueiredo, L., Ramalho, A., Oliveira, M., & Menezes, L. J. W. (2011). Experimental study of friction in sheet metal forming. *271*(9-10), 1651-1657.

Fratini, L., Pasta, S., & Reynolds, A. P. J. I. J. o. F. (2009). Fatigue crack growth in 2024-T351 friction stir welded joints: Longitudinal residual stress and microstructural effects. *31*(3), 495-500.

Frehn, A., & Bleck, W. (2003). Effect of austenite stability on the mechanical properties and delayed cracking in metastable austenitic steels. *Stainless Steel World(The Netherlands), 15*(1), 40-45.

Gangloff, R. (2003). Comprehensive Structural Integrity, Vol. by I. Milne, RO Ritchie and B. Karihaloo. In: Pergamon, San Diego.

Ginzburg, B., Shibaev, L., Kireenko, O., Shepelevskii, A., Baidakova, M., & Sitnikova, A. J. R. j. o. a. c. (2002). Antiwear effect of fullerene C 6 0 additives to lubricating oils. *75*(8), 1330-1335.

GmbH., S., & GmbH, S. (1998). *Metal forming handbook*: Springer Science & Business Media.

Gonzalez, B. M., Castro, C. S. B., Buono, V. T. L., Vilela, J. M. C., Andrade, M. S., Moraes, J. M. D. d., & Mantel, M. J. (2003). The influence of copper addition on the formability of AISI 304 stainless steel. *Materials Science and Engineering: A, 343*(1-2), 51-56.

Graber, A. (1987). Stress Corrosion Cracking of Brass Cups by Metal Forming Properties. *Metall, 41*(10), 1010-1014.

Guo, X. (2008). *Delayed cracking in high strength steels*.

Guo, X., Post, J., Groen, M., & Bleck, W. J. s. r. i. (2011). Stress Oriented Delayed Cracking Induced by Dynamic Martensitic Transformation in Meta-Stable Austenitic Stainless Steels. *82*(1), 6-13.

HÄNNINEN, H., & HAKARAINEN, T. J. C. (1980). On the effects of α′ martensite in hydrogen embrittlement of a cathodically charged AISI type 304 austenitic stainless steel. *36*(1), 47-51.

Hansen, S., & Pradhan, R. J. F. o. D.-P. S. (1981). Structure--Property Relationships and Continuous Yielding Behavior in Dual-Phase Steels. 113-144.

Hashmi, S. (2014). *Comprehensive materials processing*: Newnes.

Hauk, V. (1997). *Structural and residual stress analysis by nondestructive methods: Evaluation-Application-Assessment*: Elsevier.

Hong, S., Lee, J., Lee, S., Woo, W., Kim, S.-K., Kim, H. S. J. M., & A, M. T. (2014). Residual stress analysis in deep drawn twinning induced plasticity (TWIP) steels using neutron diffraction method. *45*(4), 1953-1961.

Hong, S., Shin, S. Y., Kim, H. S., Lee, S., Kim, S.-K., Chin, K.-G., & Kim, N. J. (2013). Effects of inclusions on delayed fracture properties of three twinning induced plasticity (TWIP) steels. *Metallurgical and Materials Transactions A, 44*(2), 776-786.

Hossain, R., Pahlevani, F., Quadir, M. Z., & Sahajwalla, V. (2016). Stability of retained austenite in high carbon steel under compressive stress: an investigation from macro to nano scale. *Scientific Reports, 6*, 34958. doi:10.1038/srep34958

Hu, Z. S., Lai, R., Lou, F., Wang, L., Chen, Z., Chen, G., & Dong, J. J. W. (2002). Preparation and tribological properties of nanometer magnesium borate as lubricating oil additive. *252*(5-6), 370-374.

Huang, G., Matlock, D., & Krauss, G. (1989). Martensite formation, strain rate sensitivity, and deformation behavior of type 304 stainless steel sheet. *Metallurgical and Materials Transactions A, 20*(7), 1239-1246.

Huang, J. (2004). *Microstructure evolution during processing of dual phase and TRIP steels.* University of British Columbia,

Huang, J., & Altstetter, C. (1991). Internal hydrogen-induced subcritical crack growth in austenitic stainless steels. *Metallurgical Transactions A, 22*(11), 2605-2618.

Hussaini, S. M., Singh, S. K., & Gupta, A. K. J. J. o. K. S. U.-E. S. (2014). Formability and fracture studies of austenitic stainless steel 316 at different temperatures. *26*(2), 184-190.

Johansson, J., Odén, M. J. M., & A, M. T. (2000). Load sharing between austenite and ferrite in a duplex stainless steel during cyclic loading. *31*(6), 1557-1570.

Jung, S. H., Lee, T., Song, S. W., Kwon, Y. J., Kang, H.-G., Chae, D., . . . Materials. (2017). Enhanced Resistance to Delayed Cracking in Deep-drawn Lean Duplex Stainless Steel: the Role of Residual Stress. *55*(8), 544-549.

Kalakada, S. B., Kumarapillai, P. N., Perikinalil, R. K. J. I. J. o. P. E., & Manufacturing. (2012). Analysis of static and dynamic performance characteristics of THD journal bearing operating under lubricants containing nanoparticles. *13*(10), 1869-1876.

Kanezaki, T., Narazaki, C., Mine, Y., Matsuoka, S., & Murakami, Y. J. I. J. o. H. E. (2008). Effects of hydrogen on fatigue crack growth behavior of austenitic stainless steels. *33*(10), 2604-2619.

Khalilpourazary, S., & Meshkat, S. J. T. I. J. o. A. M. T. (2014). Investigation of the effects of alumina nanoparticles on spur gear surface roughness and hob tool wear in hobbing process. *71*(9-12), 1599-1610.

Koo, J. (1977). *Design of duplex low carbon steels for improved strength: weight applications* (No. LBL-6657). California Univ., Berkeley (USA). Lawrence Berkeley Lab..

Kosanov, J., Lenard, J., Uhrig, J., Wallfarth, B. J. M. S., & A, E. (2006). The effect of lubricant additives on the coefficient of friction in the flat-die test. *427*(1-2), 274-281.

Kovalev, A., Wainstein, D., Mishina, V., & Zabilsky, V. J. A. I., Member/Customer Service Center, Materials Park, OH 44073-, USA, . (2002). Effect of residual stress on hydrogen embrittlement and stress corrosion cracking. 70-86.

Lai, C., Tsay, L., Chen, C. J. M. S., & A, E. (2013). Effect of microstructure on hydrogen embrittlement of various stainless steels. *584*, 14-20.

Lange, K., & Bruckner, L. (1990). Deformation-Induced Residual Stresses and Stress Corrosion in Deep-Drawn Components of Brass Materials. *Transactions of the North American Manufacturing Research Institution of SME 1990*, 71-75.

Lazarescu, L., Nicodim, I., & Banabic, D. (2015). *Evaluation of Drawing Force and Thickness Distribution in the Deep-Drawing Process with Variable Blank-Holding.* Paper presented at the Key Engineering Materials.

Lee, C.-G., Hwang, Y.-J., Choi, Y.-M., Lee, J.-K., Choi, C., Oh, J.-M. J. I. J. o. P. E., & Manufacturing. (2009). A study on the tribological characteristics of graphite nano lubricants. *10*(1), 85-90.

Lee, K., Hwang, Y., Cheong, S., Choi, Y., Kwon, L., Lee, J., & Kim, S. H. J. T. L. (2009). Understanding the role of nanoparticles in nano-oil lubrication. *35*(2), 127-131.

Lee, P.-H., Nam, J. S., Li, C., Lee, S. W. J. I. J. o. P. E., & Manufacturing. (2012). An experimental study on micro-grinding process with nanofluid minimum quantity lubrication (MQL). *13*(3), 331-338.

Lei, C., Masahide, G., Yoshiaki, H., Yukio, H. J. J. o. I., & Steel Research, I. (2007). Effect of microstructure of cementite on interphase stress state in carbon steel. *14*(4), 31-38.

Litovchenko, I. Y., Tyumentsev, A., Akkuzin, S., Naiden, E., Korznikov, A. J. T. P. o. M., & Metallography. (2016). Martensitic transformations and the evolution of the defect microstructure of metastable austenitic steel during severe plastic deformation by high-pressure torsion. *117*(8), 847-856.

Liu, G., Li, X., Qin, B., Xing, D., Guo, Y., & Fan, R. J. T. L. (2004). Investigation of the mending effect and mechanism of copper nano-particles on a tribologically stressed surface. *17*(4), 961-966.

Lo, K. H., Shek, C. H., & Lai, J. (2009). Recent developments in stainless steels. *Materials Science and Engineering: R: Reports, 65*(4-6), 39-104.

Lovell, M., Higgs, C., Deshmukh, P., & Mobley, A. J. J. o. m. p. t. (2006). Increasing formability in sheet metal stamping operations using environmentally friendly lubricants. *177*(1-3), 87-90.

Mao, C., Tang, X., Zou, H., Huang, X., Zhou, Z. J. I. J. o. P. E., & Manufacturing. (2012). Investigation of grinding characteristic using nanofluid minimum quantity lubrication. *13*(10), 1745-1752.

Martin, M., Weber, S., Izawa, C., Wagner, S., Pundt, A., & Theisen, W. J. I. J. o. H. E. (2011). Influence of machining-induced martensite on hydrogen-assisted fracture of AISI type 304 austenitic stainless steel. *36*(17), 11195-11206.

McGuire, M. F. (2008). *Stainless steels for design engineers*: Asm International.

Michler, T., Lee, Y., Gangloff, R. P., & Naumann, J. (2009). Influence of macro segregation on hydrogen environment embrittlement of SUS 316L stainless steel. *International Journal of Hydrogen Energy, 34*(7), 3201-3209.

Milititsky, M., De Wispelaere, N., Petrov, R., Ramos, J., Reguly, A., & Hänninen, H. (2008). Characterization of the mechanical properties of low-nickel austenitic stainless steels. *Materials Science and Engineering: A, 498*(1-2), 289-295.

Mosleh, M., Atnafu, N. D., Belk, J. H., & Nobles, O. M. J. W. (2009). Modification of sheet metal forming fluids with dispersed nanoparticles for improved lubrication. *267*(5-8), 1220-1225.

Narayanan, R. G. (Producer). Fundamental of modern manufacturing Materials, Processes and Systems. Retrieved from http://www.iitg.ac.in/engfac/ganu/public_html/Metal%20forming%20processes_full.pdf

Nedoseka, A. (2012). *Fundamentals of evaluation and diagnostics of welded structures*: Elsevier.

Olguner, S. and Bozdana, A.T., 2016. The effect of friction coefficient on punch load and thickness reduction in deep drawing process. *Int. J. of Materials*, *3*.Özek, C., & Bal, M. J. T. I. J. o. A. M. T. (2009). The effect of die/blank holder and punch radiuses on limit drawing ratio in angular deep-drawing dies. *40*(11-12), 1077-1083.

Pan, C., Chu, W., Li, Z., Liang, D., Su, Y., Gao, K., . . . A, E. (2003). Hydrogen embrittlement induced by atomic hydrogen and hydrogen-induced martensites in type 304L stainless steel. *351*(1-2), 293-298.

Papula, S. (2015). Delayed Cracking of Metastable Low-Nickel Austenitic Stainless Steels.

Papula, S., Saukkonen, T., Talonen, J., & Hänninen, H. J. I. I. (2015). Delayed cracking of metastable austenitic stainless steels after deep drawing. *55*(10), 2182-2188.

Papula, S., Talonen, J., Hänninen, H. J. M., & A, M. T. (2014). Effect of residual stress and strain-induced α'-martensite on delayed cracking of metastable austenitic stainless steels. *45*(3), 1238-1246.

Papula, S., Talonen, J., Todoshchenko, O., & Hänninen, H. (2014). Effect of internal hydrogen on delayed cracking of metastable low-nickel austenitic stainless steels. *Metallurgical and Materials Transactions A, 45*(11), 5270-5279.

Papula, S., Talonen, J., Todoshchenko, O., Hänninen, H. J. M., & A, M. T. (2014). Effect of internal hydrogen on delayed cracking of metastable low-nickel austenitic stainless steels. *45*(11), 5270-5279.

Patel, R., Dave, H., & Raval, H. (2015). *Study of Earing Defect during Deep Drawing Process with Finite Element Simulation.* Paper presented at the Key Engineering Materials.

Prime, M. B. (2018). The Two-Way Relationship Between Residual Stress and Fatigue/Fracture. In *Fracture, Fatigue, Failure and Damage Evolution, Volume 7* (pp. 19-23): Springer.

Prime, M. B. J. M. (2015). Training package 1 for slitting data analysis. *128*, 375-382.

Ragab, M., & Orban, H. (2000). Effect of ironing on the residual stresses in deep drawn cups. *Journal of materials processing technology, 99*(1), 54-61.

Ramezani, M., & Ripin, Z. M. (2012). *Rubber-pad forming processes: Technology and applications*: Elsevier.

Rao, K., & Xie, C. J. T. i. (2006). A comparative study on the performance of boric acid with several conventional lubricants in metal forming processes. *39*(7), 663-668.

Rapoport, L., Leshchinsky, V., Lapsker, I., Volovik, Y., Nepomnyashchy, O., Lvovsky, M., . . . Tenne, R. J. W. (2003). Tribological properties of WS2 nanoparticles under mixed lubrication. *255*(7-12), 785-793.

Rapoport, L., Leshchinsky, V., Lvovsky, M., Nepomnyashchy, O., Volovik, Y., Tenne, R. J. I. l., & tribology. (2002). Mechanism of friction of fullerenes. *54*(4), 171-176.

Rastogi, R., Yadav, M., & Bhattacharya, A. J. W. (2002). Application of molybdenum complexes of 1-aryl-2, 5-dithiohydrazodicarbonamides as extreme pressure lubricant additives. *252*(9-10), 686-692.

Reddy, R. V., Reddy, T., Reddy, G. J. I. J. o. E. T., & Technology. (2012). Optimization of blank holder force to control wrinkling and fracture of cylindrical cups in deep drawing. *3*(5), 669-676.

Wagoner, R. H., & Chenot, J. L. (1996). *Fundamentals of metal forming*. John Wiley & Sons Inc.

Robertson, I. J. E. F. M. (1999). The effect of hydrogen on dislocation dynamics. *64*(5), 649-673.

Saito, K., & Shimahashi, Y. (1979). *Residual stresses in deep drawn cups and sunk tubes.* Paper presented at the Metal Forming Plasticity\ Proc. Conf.\, Tutzing, Germany, Aug.-Sept. 1978.

San Marchi, C., Somerday, B., Tang, X., & Schiroky, G. J. I. J. o. H. E. (2008). Effects of alloy composition and strain hardening on tensile fracture of hydrogen-precharged type 316 stainless steels. *33*(2), 889-904.

SANIEE, F., PILLINGER, I., & HARTLEY, P. (2004). FRICTION MODELLING FOR THE PHYSICAL SIMULATION OF THE BULK METAL FORMING PROCESSES.

Saravanakumar, N., Prabu, L., Karthik, M., Rajamanickam, A. J. J. o. M. S., & Technology. (2014). Experimental analysis on cutting fluid dispersed with silver nano particles. *28*(2), 645-651.

Schey, J. A. (1987). *Introduction to manufacturing processes* (Vol. 2): McGraw-Hill New York etc.

Schey, J. A. J. L., & wear. (1983). Tribology in metalworking: Friction. 451.

Sibanda, M., Vismer, S., & Knutsen, R. (1994). Consideration of reduced nickel containing austenitic stainless steels for forming applications. *Materials Letters, 21*(2), 203-207.

Siebel, E., & Kotthaus, H. (1954). Investigation of the effect of the clearance on the deformation and residual stresses by deep drawing. *Mitt. Forschungsgesellschaft f. Blechverarbeitung (8)*, 85-89.

Simmons, J. (1996). Overview: high-nitrogen alloying of stainless steels. *Materials Science and Engineering: A, 207*(2), 159-169.

Simões, V. M. N. (2012). *Analysis of the influence of process parameters in the deep drawing of a cylindrical cup.*

Sniekers, R. J. P., Technische Universiteit Eindhoven, Netherlands. (1996). Friction in deep drawing.

Sondur, D., Kabadi, V., & Mallapur, D. J. P. M. S. (2014). Influence of martensite phase on the tribological properties of plain carbon steel. *5*, 464-471.

Sudo, M., Iwase, T., Hattori, Y., & Nakajima, M. (2005). *Residual stresses due to deep-drawing of pre-coated aluminum-alloy sheets.* Paper presented at the Materials Science Forum.

Sumitomo, H. (1987). Earing and delayed cracking of deep-drawn cup of austenitic stainless steel sheets. *Advanced Technology of Plasticity 1987., 2*, 1289-1296.

Suzuki, T., Kojima, H., Suzuki, K., Hashimoto, T., & Ichihara, M. J. A. M. (1977). An experimental study of the martensite nucleation and growth in 18/8 stainless steel. *25*(10), 1151-1162.

Talonen, J. (2007). A Doctoral Thesis. *Helsinki University of Technology, Espoo, Finland*.

Talonen, J. (2007). Effect of strain-induced α'-martensite transformation on mechanical properties of metastable austenitic stainless steels.

Tan, C., Aslian, A., Abe, Y., & Mori, K. (2016). Improved seizure resistance of ultra-high-strength steel ironed cups with a lubricant containing SiO2 nanoparticles. *The International Journal of Advanced Manufacturing Technology, 87*(5-8), 1705-1711.

Tan, C.J., Abe, Y., Daodon, W., Takahashi, N., Mori, K. and Purbolaksono, J., 2016. Increase in ironing limit of aluminium alloy cups with lubricants containing nanoparticles. *Journal of Materials Processing Technology*, *229*, pp.804-813.

Tao, X., Jiazheng, Z., & Kang, X. J. J. o. P. D. A. P. (1996). The ball-bearing effect of diamond nanoparticles as an oil additive. *29*(11), 2932.

Taran, Y. V., Daymond, M., & Schreiber, J. J. P. B. C. M. (2004). Interplay of stresses induced by phase transformation and plastic deformation during cyclic load of austenitic stainless steel. *350*(1-3), 98-101.

Teus, S., Shyvanyuk, V., & Gavriljuk, V. (2008). Hydrogen-induced γ→ ε transformation and the role of ε-martensite in hydrogen embrittlement of austenitic steels. *Materials Science and Engineering: A, 497*(1), 290-294.

Thakre, A. A., Thakur, A. J. I. L., & Tribology. (2015). Study of behaviour of aluminium oxide nanoparticles suspended in SAE20W40 oil under extreme pressure lubrication. *67*(4), 328-335.

Thirumalaikumaran, A. J. I. R. J. o. E., & e-ISSN, T. (2017). The Tribological Behaviour of Nanoparticles Mixed Lubricating Oil–Review. 2395-0056.

Thottackkad, M. V., Perikinalil, R. K., Kumarapillai, P. N. J. I. j. o. p. e., & manufacturing. (2012). Experimental evaluation on the tribological properties of coconut oil by the addition of CuO nanoparticles. *13*(1), 111-116.

Todinov, M. T. (2006). *Risk-based reliability analysis and generic principles for risk reduction*: Elsevier.

Wang, W., Su, Y., Yan, Y., Li, J., Qiao, L., Chu, W., . . . Xing, Y. J. C. S. (2012). The role of hydrogen in stress corrosion cracking of 310 austenitic stainless steel in a boiling MgCl2 solution. *60*, 275-279.

Wang, Z., & Gong, B. (2002). Residual stress in the forming of materials. *Handbook of residual stress and deformation of steel*, 141-149.

Wilson, W., Hsu, T., & Huang, X. J. J. o. e. f. i. (1995). A realistic friction model for computer simulation of sheet metal forming processes. *117*(2), 202-209.

Withers, P. J., Bhadeshia, H. J. M. s., & Technology. (2001). Residual stress. Part 1– measurement techniques. *17*(4), 355-365.

Wu, Y.-Y., Kao, M.-J. J. I. L., & Tribology. (2011). Using TiO2 nanofluid additive for engine lubrication oil. *63*(6), 440-445.

Xiaodong, Z., Xun, F., Huaqiang, S., & Zhengshui, H. J. L. S. (2007). Lubricating properties of Cyanex 302-modified MoS2 microspheres in base oil 500SN. *19*(1), 71-79.

Yang, T. J. T. I. (2010). Investigation of the strain distribution with lubrication during the deep drawing process. *43*(5-6), 1104-1112.

Yang, Y., Xu, H., & Xing, Z. (1990). *Study of longitudinal cracking of drawn austenitic stainless steel vessels.* Paper presented at the IDDRG Working Group Meetings: Material.

Ye, L. (2015). *Recent Advances in Structural Integrity Analysis-Proceedings of the International Congress (APCF/SIF-2014):(APCFS/SIF 2014)*: Woodhead Publishing.

Yoshimura, H., Torikai, S., Nishihara, T., Nonishi, T., & Inouchi, N. J. J. o. m. p. t. (2002). Application of wheat flour lubricants to the press-forming process. *125*, 375-378.

Yuying, Y., Chunfeng, L., & Hongzhi, X. (1992). A study of longitudinal cracking and the forming technology for deep-drawn austenitic stainless-steel cups. *Journal of materials processing technology, 30*(2), 167-172.

Zaid, A. I. (2016). *Deep drawing mechanism, parameters, defects and recent results: state of the art.* Paper presented at the IOP Conference Series: Materials Science and Engineering.

Zareh-Desari, B., Abaszadeh-Yakhforvazani, M., Khalilpourazary, S. J. I. J. o. P. E., & Manufacturing. (2015). The effect of nanoparticle additives on lubrication performance in deep drawing process: Evaluation of forming load, friction coefficient and surface quality. *16*(5), 929-936.

Zhang, G., Chang, L., Schlarb, A. J. C. S., & Technology. (2009). The roles of nano-SiO2 particles on the tribological behavior of short carbon fiber reinforced PEEK. *69*(7-8), 1029-1035.

Zhang, L., Imade, M., An, B., Wen, M., Iijima, T., Fukuyama, S., & Yokogawa, K. (2012a). Internal reversible hydrogen embrittlement of austenitic stainless steels based on type 316 at low temperatures. *ISIJ international, 52*(2), 240-246.

ZHANG, L., IMADE, M., AN, B., WEN, M., IIJIMA, T., FUKUYAMA, S., & YOKOGAWA, K. J. I. i. (2012b). Environmental degradation of engineering materials in hydrogen Environmental degradation of engineering materials in hydrogen 283, 1981. *52*(2), 240-246.

Zhang, L., Imade, M., An, B., Wen, M., Iijima, T., Fukuyama, S., & Yokogawa, K. J. I. i. (2012c). Internal reversible hydrogen embrittlement of austenitic stainless steels based on type 316 at low temperatures. *52*(2), 240-246.

Zhang, L., Wen, M., Imade, M., Fukuyama, S., & Yokogawa, K. J. A. M. (2008). Effect of nickel equivalent on hydrogen gas embrittlement of austenitic stainless steels based on type 316 at low temperatures. *56*(14), 3414-3421.

Zhou, J., Wu, Z., Zhang, Z., Liu, W., & Dang, H. J. W. (2001). Study on an antiwear and extreme pressure additive of surface coated LaF3 nanoparticles in liquid paraffin. *249*(5-6), 333-337.

Zinbi, A., & Bouchou, A. (2010). Hydrogen-induced delayed cracking in the AISI 301 unstable austenitic steel sheet. *Materials & Design, 31*(8), 3989-3995.

Zinbi, A., & Bouchou, A. J. E. F. A. (2010). Delayed cracking in 301 austenitic steel after bending process: martensitic transformation and hydrogen embrittlement analysis. *17*(5), 1028-1037.